Analytical Biochemistry 385 (2009) 138–142

Contents lists available at ScienceDirect

Analytical Biochemistry

journal homepage: www.elsevier.com/locate/yabio

A microfluidic dual capillary probe to collect messenger RNA from adherent cells and spheroids

Hitoshi Shiku [a,*], Takeshi Yamakawa [a], Yuji Nashimoto [a], Yasufumi Takahashi [a], Yu-suke Torisawa [a], Tomoyuki Yasukawa [a], Takahiro Ito-Sasaki [b], Masaki Yokoo [c], Hiroyuki Abe [b], Hideki Kambara [d,e], Tomokazu Matsue [a,*]

[a] Graduate School of Environmental Studies, Tohoku University, Aobe 6-6-11-604, Sendai 980-8579, Japan
[b] Graduate School of Science and Engineering, Yamagata University, Yonezawa 992-8510, Japan
[c] Innovation of New Biomedical Engineering Center, Tohoku University, Sendai 980-8574, Japan
[d] Central Research Laboratory, Hitachi, Kokubunji, Tokyo 185-8601, Japan
[e] Tokyo University of Agriculture and Technology, Koganei, Tokyo 184-8588, Japan

ARTICLE INFO

Article history:
Received 3 September 2008
Available online 5 November 2008

Keywords:
RT-PCR
Real-time PCR
Microfluidics
Single cell analysis

ABSTRACT

Collection of bioanalytes from single cells is still a challenging technology despite the recent progress in many integrated microfluidic devices. A microfluidic dual capillary probe was prepared from a theta (θ)-shaped glass capillary to analyze messenger RNA (mRNA) from adherent cells and spheroids. The cell lysis buffer solution was introduced from the injection aperture, and the cell-lysed solution from the aspiration aperture was collected for further mRNA analysis based on reverse transcription real-time PCR. The cell lysis buffer can be introduced at any targeted cells and never spilled out of the targeted area by using the microfluidic dual capillary probe because laminar flow was locally formed near the probe under the optimized injection/aspiration flow rates. This method realizes the sensitivity of mRNA at the single cell level and the identification of the cell types on the basis of the relative gene expression profiles.

Hydrodynamics is an important aspect for controlling the mass transfer of reagents and has been combined with various analytical tools such as electrochemical [1–5], electrophoretic [6–8], and chromatographic [9] instruments. Recently, the concept of a micro-total analysis system (μTAS)[1] has been receiving attention in analytical chemistry to realize integration of parallel and sequential operations on a solid substrate [10–13]. Microfluidic devices have rendered possible the guiding of chemicals based on laminar flow [14–18]. This technology has been applied for local patterning of proteins [14], targeted delivery of cells, and removal of attached cells [15,16]. However, for most chip designs, microfluidics has currently been constructed in "closed" channels based on the lab-on-a-chip concept. Delamarche and coworkers invented the remarkably innovative microfluidic probe (MFP) that can be applied in "open" space and, therefore, can form a focused laminar flow at any site for protein patterning, cell lysing, and injecting fluorescent dyes into target cells [19,20]. The original MFP possessed a mesa structure prepared with a silicon chip and two apertures for injection and aspiration.

In the current study, we first applied the MFP technology for collection of messenger RNA (mRNA) from single adherent cells. The probe has been constructed with a dual pipette and comprised a theta (θ)-shaped glass capillary. Pulled glass capillaries [21–24] and dual pipette probes [25–30] have been used in various analytical tools with micromanipulators, including physiology, capillary electrophoresis, and electrochemistry, as well as for various scanning probe microscopies (SPMs). An exclusive characteristic of MFP allows the aspirated sample solution to be used for further analysis, similar to that in perfusion or microdialysis. We collected mRNA from monolayer-cultured cells, namely the human breast cancer cell line MCF-7 and the malignant human mammary epithelial cell line HMT-3522 T4-2 (T4-2) [31,32], using the probe for injecting a lysis buffer and aspirating the lysed cytosol. The collection efficiency of the mRNA was evaluated quantitatively using real-time PCR. This technique has a significant impact in the research field of single cell analysis because the collection process is the bottleneck to automatically perform sequential chemical processing on an integrated μTAS device. We focused on the expression levels of β1-integrin, a major protein to regulate cell–cell and cell–ECM (extracellular matrix) interactions, because the microfluidic dual capillary probe is principally applicable to collect

* Corresponding authors. Fax: +81 22 217 7209.
E-mail addresses: shiku@bioinfo.che.tohoku.ac.jp (H. Shiku), matsue@bioinfo.che.tohoku.ac.jp (T. Matsue).

[1] *Abbreviations used:* μTAS, micro-total analysis system; MFP, microfluidic probe; mRNA, messenger RNA; SPM, scanning probe microscopy; T4-2, HMT-3522 T4-2; ECM, extracellular matrix; DMEM, Dulbecco's modified Eagle's medium; PCR, polymerase chain reaction; RNase, ribonuclease; RT, reverse transcription; cDNA, complementary DNA; GAPDH, glyceraldehyde-3-phosphate dehydrogenase.

0003-2697/$ - see front matter © 2008 Elsevier Inc. All rights reserved.
doi:10.1016/j.ab.2008.10.039

adherent cells and spheroids at any position. It is already known that β1-integrin expression for MCF-7 is significantly smaller than that for T4-2. Also, it is known that β1-integrin expression for spheroid culture is larger than that for monolayer culture. Therefore, as a model system, MCF-7 and T4-2 cell lines cultured in monolayer and spheroid cultures were selected for the mRNA analysis samples.

Materials and methods

Microfluidic dual capillary probe

A theta-shaped borosilica glass tube (1.5 mm o.d., 1.02 mm i.d., TST150-6, World Precision Instruments) was cut to a length of 50 mm and pulled with a capillary puller (PN-3, Narishige). The top of the dual pipette capillary was then planed with a diamond grinder (EG-6, Narishige) to fabricate a disk-shaped tip with an outer diameter of 40 to 100 μm (Fig. 1). It was difficult to prepare the probes with precisely the same orifice size.

The bottom of the dual pipette probe was connected to the two silica capillary tubes (25 cm in length, 0.375 mm o.d., 0.075 mm i.d., 31942, GL Science) by using epoxy glue. The two microsyringes, syringe 1 (used for injection) and syringe 2 (used for aspiration), were connected tightly with the silica capillary tube with a special adaptor set (Upchurch Scientific).

Cell culture

Methods for monolayer culture [33] and three-dimensional culture on reconstructed basement membrane (on-top culture) [34] have been described elsewhere [35]. The human breast cancer cell line (MCF-7) was donated by the Cell Resource Center for Biomedical Research (Tohoku University). The malignant human mammary epithelial cell line (T4-2) [32] was obtained from the American Type Culture Collection. RPMI 1640 medium (Gibco) containing 10% fetal bovine serum (FBS, Gibco), 50 μg ml^{-1} penicillin (Gibco), and 50 μg ml^{-1} streptomycin (Gibco) was used for MCF-7 culture. Dulbecco's modified Eagle's medium (DMEM)/F12 medium (Gibco) containing 250 ng ml^{-1} insulin (Boehringer Mannheim), 10 μg ml^{-1} transferrin (Sigma), 2.6 ng ml^{-1} sodium selenite (Collaborative Research), 0.1 nM estradiol (Sigma), 1.4 μM hydrocortisone (Collaborative Research), and 5 μg ml^{-1} prolactin (Sigma) was used for culturing T4-2. For monolayer culture, The bottom of a 35-mm polystyrene culture dish (BD Biosciences) was coated with type 1 collagen solution (Research Institute for the Functional Peptides) by incubation for more than 30 min. Cells were seeded onto the collagen-coated dish as a single cell suspension. For on-top culture, the bottom of a 35-mm polystyrene culture dish was initially coated with 30 μl of Matrigel (BD Biosciences). The Matrigel coated on the culture dish was solidified at 37 °C for 10 min. Single cells were seeded on the layer of the Matrigel with 50 μl of 1 to 5 × 10^4 cells/ml cell suspension in medium solution containing 2% Matrigel. Single cells were adherent onto the Matrigel layer after 30 to 60 min incubation at 37 °C. The culture dish was further filled with the medium containing 2% Matrigel. Cells proliferate and form spheroids after 3 days.

Cell lysis and mRNA collection with the microfluidic dual capillary probe

The probe was silanized with a 50-μl drop of 4,4,5,5,6,6,6-nonafluorohexyltrichlorosilane (LS-912, Shin-etsu Chemical) evaporated in a closed 200-ml beaker under a nitrogen atmosphere at room temperature for 2 h. The probe and the two syringes were washed with 99.6% ethanol. The probe was set on an XYZ stage, and the two syringes were controlled with syringe pumps (KDS200&KDS230, Muromachi). The distance between the probe and the sample was defined by gently touching the bottom of the culture dish, and the probe was retracted 20 μm apart from the bottom using a motor-driven XYZ stage and a stage controller (D73MS, Suruga Seiki). Then the probe was located at the center of the microscope view.

Cell extraction using microfluidic dual capillary probe

Fig. 1 shows a scheme of the experimental setup. The lysis buffer RLT (50 μl, RNeasy Micro Kit, Qiagen) was roared into the injection syringe (syringe 1) and the aspiration syringe (syr-

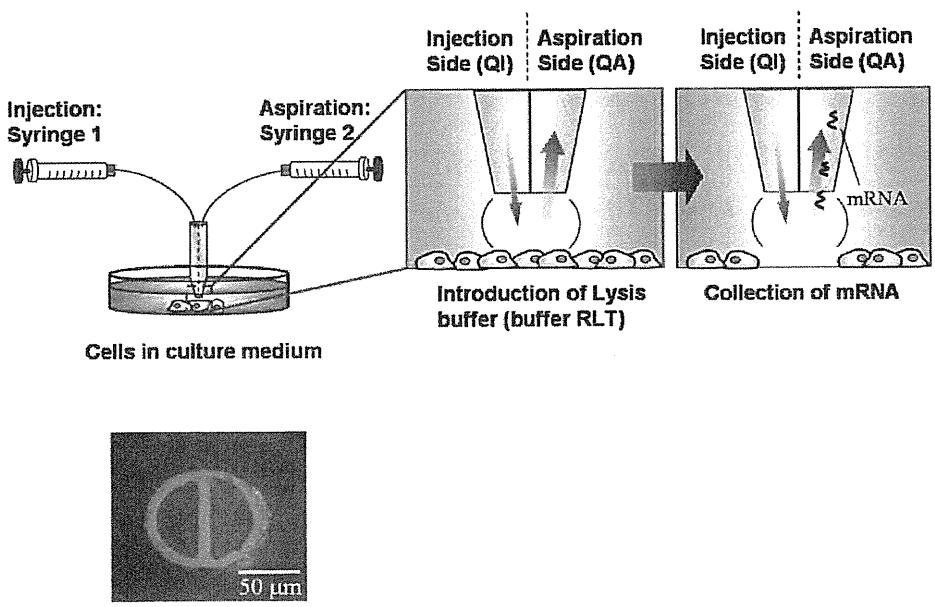

Fig. 1. Scheme of the experimental setup. QI (injection flow rate) and QA (aspiration flow rate) were set at 40 and 360 nl/min, respectively. The flow rate ratio (QA/QI) was set at 9. A bottom view of the theta-shaped microfluidic dual capillary probe is also shown.

inge 2). mRNA was collected from MCF-7 monolayer cells by using the microfluidic dual capillary probe. The injection (QI) and aspiration (QA) flow rates were set at 40 and 360 nl/min, respectively. The flow rate ratio (QA/QI) was 9 [19]. After the observation of cellular lysis and removal from the culture dish, the probe was transferred into another dish filled with 2 ml of buffer RLT and further aspirated at 5 μl/min for 10 min. Initially, syringe 2 was loaded with 50 μl of buffer RLT; thus, the final volume of the collected cell-lysed solution with syringe 2 resulted in approximately 150 μl. The collected cell lysate solution was poured out into a 0.2-ml polymerase chain reaction (PCR) tube. Then 5 μl of the 4 ng/μl carrier RNA (Qiagen) was added into the PCR tube for preventing the degradation of the targeted RNA originating from contaminated ribonuclease (RNase). The carrier RNA also guards the adsorption of the targeted RNA onto the PCR tube.

The solution in the PCR tube was then purified using an RNeasy Micro Kit (Qiagen). Reverse transcription (RT) reaction and real-time PCR were performed using a QuantiTect Reverse Transcription Kit (Qiagen) and a LightCycler FastStart DNA Master Kit (Roche), respectively. The real-time PCR (LightCycler 1.5, Roche) was performed for at least two genes using 2 μl of the sample complementary DNA (cDNA) taken from 20 μl of the synthesized source cDNA solution. The running conditions have been described elsewhere [35]. Primers for glyceraldehyde-3-phosphate dehydrogenase (GAPDH, GenBank Accession No. M33197) and β1-integrin (GenBank Accession No. NM_133376) were designed and synthesized by Nihon Gene Research Laboratories. The actual sequences, apricon sizes, and annealing temperatures of the primers were listed as follows: GAPDH, forward 5′-TGA ACG GGA AGC TCA CTG G-3′, reverse 5′-TCC ACC ACC CTG TTG CTG TA-3′, 307 bp, 62 °C; β1-integrin, forward 5′-GTC CAA CCT GAT CCT GTG TC-3′, reverse 5′-GCA ACC ACA CCA GCT ACA AT-3′, 167 bp, 66 °C. The precise GAPDH copy number was determined using a standard plasmid DNA-containing GAPDH synthesized by Nihon Gene Research Laboratories. We also performed bulk measurement using 10^5 to 10^6 cells as a starting sample. In this case, an RNeasy Mini Kit (Qiagen) was used for RNA purification. For the monolayer cultured cell sample, the medium (RPMI 1640 or DMEM/F12) of the culture dish was changed to the cell lysis buffer RLT (Quiagen), and the lysate was further analyzed to estimate the relative β1-integrin expression level normal to GAPDH for each cell type. The process for spheroid lysis and mRNA extraction was basically the same as that for the monolayer adherent cells.

Results and discussion

Fig. 2A shows the sequential photographs of the sample MCF-7 monolayer cultured on a 35-mm polystyrene dish before and after the cellular collection using the dual capillary probe at a probe–sample distance of 20 μm. Initially, syringe 2 was turned on to aspirate the culture medium from aperture 2 at a flow rate of 360 nl/min (QA). Syringe 1 was immediately used to inject the cell lysis buffer from aperture 1 at a flow rate of 40 nl/min (QI). This protocol ensured that cell lysis buffer solution never spilled out of the targeted area. As seen in Fig. 2A, the target cells were removed within 30 s and the number of lysed cells was found to be 11. The margins of the removed cells are nearly intact, ensuring that the cell lysis buffer attacks only the targeted area during laminar flow when introduced and never leaks out of the targeted area. In the same manner, one cell collection was demonstrated from adherent MCF-7 cells seeded with a lower cellular density (Fig. 2B).

Fig. 3 shows the time course during the real-time PCR operation and the melting curve analysis performed after the real-time PCR for β1-integrin mRNA sample collected from MCF-7 monolayer. These results were obtained from 11 cells and 1 cell using the microfluidic dual capillary probe corresponding to the photographs shown in Fig. 2A and B, respectively. The peak in the melting curve was well correlated with the signal obtained for the bulk of cellular samples with 10^5 to 10^6 cells.

The copy number of the GAPDH, which was collected from the MCF-7 monolayer (including 1–17 cells, $n = 6$) by using the probe, was 76.7 copies/cell. This value corresponded to the apparent collection efficiency 7.6% because the copy number estimated using bulk measurement ($\sim 10^6$ cells) was 1014 copies/cell. This low efficiency is due to the instability of the mRNA; the expected collection efficiency with QA/QI = 9 was approximately 100%, as shown in the literature [19]. In our case, the collection efficiency of approximately 100% was achieved for a QA/QI value larger than 8 when a solution containing 10^5 particles/ml of 6-μm-diameter microspheres (Polysciences) was introduced through the microfluidic dual capillary probe. The concentration of the product (mRNA) should be high; thus, the QA/QI value cannot be set at an undesirably larger value for our objective, that is, mRNA collection. The smaller the gap distance becomes, the larger the expected collection efficiency increases. The orifice size did not seem to affect the collection efficiency of the mRNA. The microfluidic dual capillary probe with less than 10 μm diameter can be fabricated, and we observed that a part of the MCF-7 spheroid was lysed with the smaller probe. However, in the current stage, we have not succeeded in RNA analysis with the smaller probe.

The retention time of the cell-lysed solution including mRNA and buffer RLT within the aspiration side compartment of the probe is 38 min, which is estimated from the volume of the aspiration side compartment (13.7 μl, a half-volume of the dual capillary probe) and the QA value (360 nl/min). This time scale is significantly large compared with the actual time period taken for the process of cell lysis (30 s), implying that the collected mRNA remains in the probe compartment but does not reach syringe 2. During the cell lysis, buffer RLT is diluted to approximately 10% of the original concentration, and this may be the main reason for the mRNA degradation given the roles that buffer RLT plays in RNase deactivation and RNA stabilization. After the cell lysis process, the probe was transferred into a buffer RLT pool and further aspirated with 50 μl (see Materials and Methods). In this step, the cell-lysed sample surely reaches syringe 2, where the concentration of buffer RLT recovers to the original one because the volume of the cell-lysed sample (180 nl) is negligibly small compared with the total volume of buffer RLT (150 μl).

Although the mRNA collection efficiency was low in the current stage, comparison of the gene expression at individual cell level was possible. Expression of β1-integrin for MCF-7 and T4-2 collected using the microfluidic dual capillary probe was surveyed normal to that of GAPDH for each. Fig. 4 reveals the relative β1-integrin expression for a small number of adherent cells (1 to 17 MCF-7 cells [$n = 6$] and 1 T4-2 cell [$n = 3$] cultured with monolayer). The β1-integrin expression for the T4-2 cells was approximately 10-fold greater than that for the MCF-7 cells. The results obtained using the current method with the microfluidic dual capillary probe are similar to those obtained using a conventional method based on the collection of bulk cells ($\sim 10^6$ cells), indicating that the current method provided quantitative information regarding the expression levels of the target gene in the two cell lines. T4-2 expresses β1-integrin at substantially higher level than does MCF-7 [31]. Although our theta-shaped probe was very easy to fabricate, the performance was comparable to that achieved by a sophisticated MFP [19].

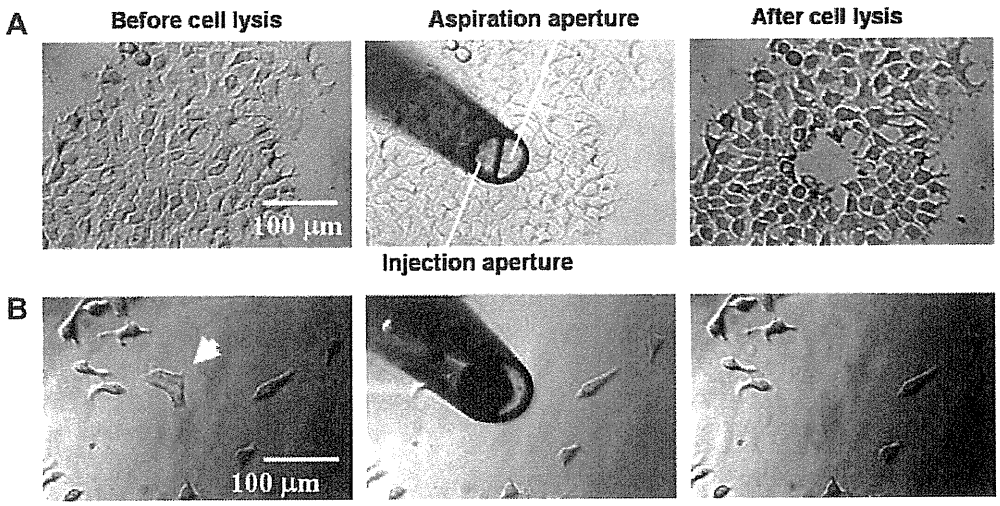

Fig. 2. (A) Sequential photos of MCF-7 monolayer before and after the RNA collection using the microfluidic dual capillary probe. The injection (QI) and aspiration (QA) flow rates were set at 40 and 360 nl/min, respectively. The distance between the probe and the bottom of the culture dish was set at 20 μm. It takes 10 to 30 s for the cell lysis to be completed, and the total volume of the cell-lysed solution was approximately 150 μl. From this picture, 11 cells were collected to further mRNA analysis. (B) In the same manner, the single cell collection was available from adherent MCF-7 cells seeded with a lower cellular density.

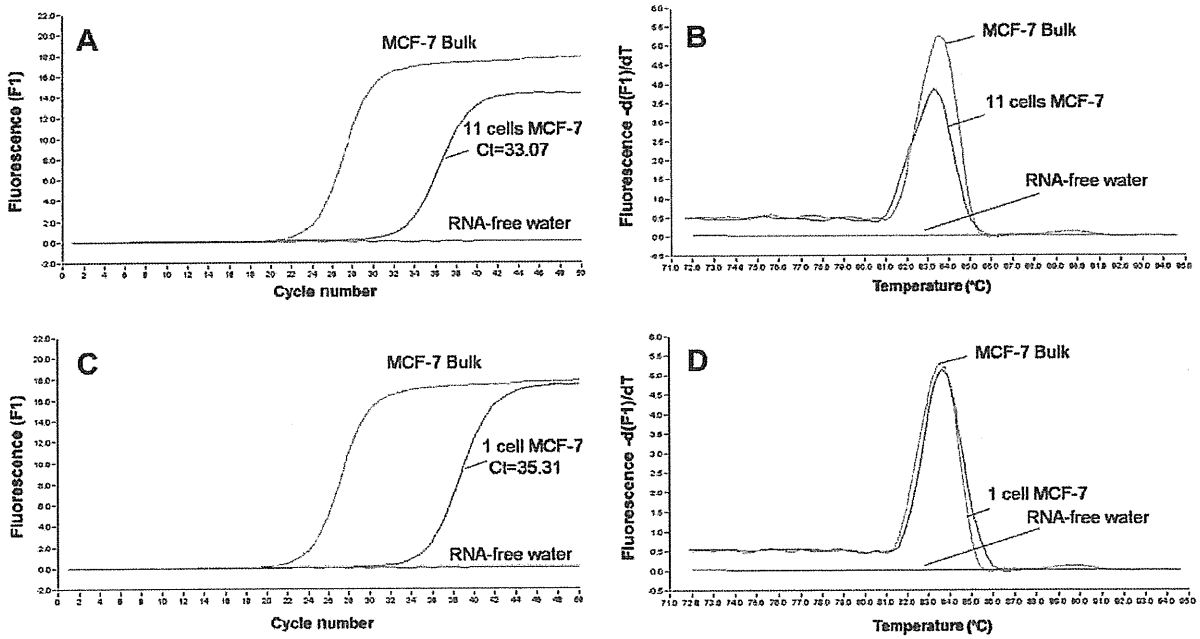

Fig. 3. Time course of the fluorescence intensity during the real-time PCR operation (A and C) and melting curve analysis performed after real-time PCR (B and D) for the β1-integrin mRNA sample collected from MCF-7 monolayer (11 cells [A and B] and 1 cell [C and D] shown in Fig. 2) using the microfluidic dual capillary probe.

Moreover, our method enabled collection of mRNA from a single spheroid, namely, an aggregated cellular mass in a three-dimensional cultures system. MCF-7 and T4-2 cells were cultured onto a Matrigel sheet to form a spheroid 3 days after the single cell seeding. Initially, we tried to pick one cell or several cells from a spheroid using the microfluidic dual capillary probe, but it was difficult to lyse a part of the single spheroid with a diameter of 100 μm. Fig. 5 shows the relative β1-integrin expression from single spheroids (MCF-7 [$n = 4$] and T4-2 [$n = 2$]). The β1-integrin expression for the spheroid was identical to, or a little bit larger than, that cultured with monolayer for both cell types. The results obtained for bulk measurement (~8000 spheroids) were in good agreement with those obtained for individual spheroids collected using the theta-shaped probe. Again, the results of the relative gene expression profiles clearly identified the differences between the two cell types.

Conclusions

In conclusion, MFP technology has been applied, for the first time, for the mRNA collection and analysis of single adherent cells and single spheroids. The collection efficiency was estimated as 7.6% using the GAPDH mRNA from single MCF-7 cells. Using the current method, a quantitative discussion is possible to distinguish

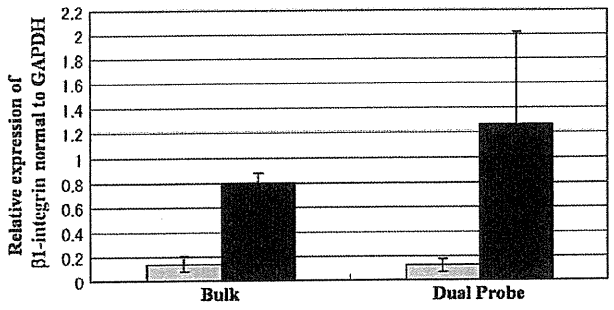

Fig. 4. Relative expression levels of β1-integrin normal to GAPDH for MCF-7 cells (gray bars) and T4-2 cells (filled bars) cultured with monolayer. mRNA collected from bulk (~10^6 cells) (left) and the microfluidic dual capillary probe (right).

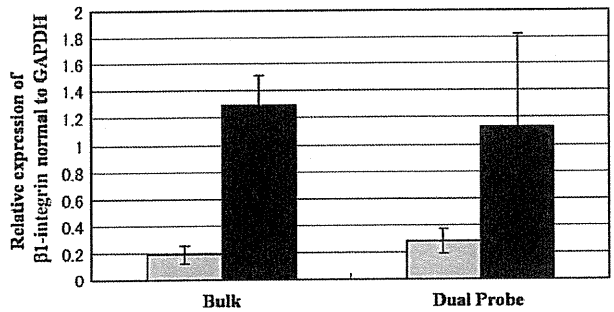

Fig. 5. Relative expression levels of β1-integrin normal to GAPDH in spheroids for MCF-7 cells (gray bars) and T4-2 cells (filled bars) three-dimensionally cultured for 3 days onto a Matrigel sheet. mRNA was collected from bulk (~8000 spheroids) (left) and the microfluidic dual capillary probe (1 spheroid) (right).

the difference in the gene expression levels between the two cell lines: MCF-7 and T4-2. The current method is also applicable to mRNA analysis in a three-dimensional culture system.

Acknowledgments

This work was supported partly by a Grant-in-Aid for Scientific Research on Priority Areas (445), "Life Surveyor," from the Ministry of Education, Culture, Sports, Science, and Technology (MEXT) of Japan; by Grants-in-Aid for Scientific Research (18101006 and 19750055) from MEXT; and by a research grant from the Center for Interdisciplinary Research at Tohoku University.

References

[1] P.R. Unwin, Dynamic electrochemistry as a quantitative probe of interfacial physicochemical processes, J. Chem. Faraday Trans. 94 (1998) 3183–3195.
[2] J.V. Macpherson, P.R. Unwin, Hydrodynamic modulation voltammetry with an oscillating microjet electrode, Anal. Chem. 71 (1999) 4642–4648.
[3] O. Niwa, R. Kurita, Z. Liu, T. Horiuchi, K. Torimitsu, Subnanoliter volume wall-jet cells combined with interdigitated microarray electrode and enzyme modified planar microelectrode, Anal. Chem. 72 (2000) 949–955.
[4] A. Aoki, T. Matsue, I. Uchida, Electrochemical response at microarray electrodes in flowing streams and determination of catecholamines, Anal. Chem. 62 (1990) 2206–2210.
[5] T. Matsue, A. Aoki, E. Ando, I. Uchida, Multichannel electrochemical detection system for flow analysis, Anal. Chem. 62 (1990) 407–409.
[6] H. Kambara, S. Takahashi, Multiple-sheathflow capillary array DNA analyzer, Nature 361 (1993) 565–566.
[7] S. Takahashi, K. Murakami, T. Anazawa, H. Kambara, Multiple sheath-flow gel capillary-array electrophoresis for multicolor fluorescent DNA detection, Anal. Chem. 66 (1994) 1021–1026.
[8] C.E. Lunte, P.T. Kissinger, R.E. Shoup, Difference mode detection with thin-layer dual-electrode liquid chromatography/electrochemistry, Anal. Chem. 57 (1985) 1541–1546.
[9] R.T. Kennedy, M.D. Oates, B.R. Cooper, B. Nickerson, J.W. Jorgenson, Microcolumn separations and the analysis of single cells, Science 246 (1989) 57–63.
[10] C.E. Sims, N.L. Allbritton, Analysis of single mammalian cells on-chip, Lab Chip 7 (2007) 423–440.
[11] P.S. Dittrich, K. Tachikawa, A. Manz, Micro total analysis systems: Latest advancements and trends, Anal. Chem. 78 (2006) 3887–3907.
[12] G. Jiang, D.J. Harrison, MRNA isolation in a microfluidic device for eventual integration of cDNA library construction, Analyst 125 (2000) 2176–2179.
[13] G.M. Whitesides, The origins and the future of microfluidics, Nature 442 (2006) 368–373.
[14] E. Delamarche, A. Bernard, H. Schmid, B. Michel, H. Biebuyck, Patterned delivery of immunoglobulins to surfaces using microfluidic networks, Science 276 (1997) 779–781.
[15] S. Takayama, J.C. McDonald, E. Otsuni, M.N. Liang, P.J.A. Kenis, R.F. Ismagilov, G.M. Whitesides, Patterning cells and their environments using multiple laminar fluid flows in capillary networks, Proc. Natl. Acad. Sci. USA 96 (1999) 5545–5548.
[16] Y.C. Tung, Y.S. Torisawa, N. Futai, S. Takayama, Small volume low mechanical stress cytometry using computer-controlled Braille display microfluidics, Lab Chip 7 (2007) 1497–1503.
[17] H. Kaji, M. Nishizawa, T. Matsue, Localized chemical stimulation to micropatterned cells using multiple laminar fluidic flows, Lab Chip 3 (2003) 208–211.
[18] A.M. Taylor, M. Blurton-Jones, S.W. Rhee, D.H. Criccs, C.W. Cotman, N.L. Jeon, A microfluidic culture platform for CNS axonal injury, Regen. Trans. Nat. Methods 2 (2005) 599–605.
[19] D. Juncker, H. Schmid, E. Delamarche, Multipurpose microfluidic probe, Nat. Mater. 4 (2005) 622–628.
[20] E. Delamarche, D. Juncker, H. Schmid, Microfluidics for processing surfaces and miniaturizing biological assays, Adv. Mater. 17 (2005) 2911–2933.
[21] A. Bruckbauer, D. Zhou, L. Ying, Y.E. Korchev, C. Abell, D. Klenerman, Multicomponent submicron features of biomolecules created by voltage controlled deposition from a nanopipet, J. Am. Chem. Soc. 125 (2003) 9834–9839.
[22] J. Olfosson, M. Levin, A. Stromberg, S.G. Weber, F. Rytten, O. Orwar, Scanning electroporation of selected areas of adherent cell cultures, Anal. Chem. 79 (2007) 4410–4418.
[23] Y. Takahashi, Y. Hirano, T. Yasukawa, H. Shiku, H. Yamada, T. Matsue, Topographic, electrochemical, and optical images using standing approach mode scanning electrochemical/optical microscopy, Langmuir 22 (2006) 10299–10306.
[24] A.D. Modestov, S. Srebnik, O. Lev, J. Gun, Scanning capillary microscopy/mass spectrometry for mapping spatial electrochemical activity of electrodes, Anal. Chem. 73 (2001) 4229–4240.
[25] K.T. Rodolfa, A. Bruckbauer, D. Zhou, Y.E. Korchev, D. Klenerman, Two-component graded deposition of biomolecules with double-barreled nanopipette, Angew. Chem. Intl. Ed. 44 (2005) 6854–6859.
[26] K.T. Rodolfa, A. Bruckbauer, D. Zhou, A.I. Schevchuk, Y.E. Korchev, D. Klenerman, Nanoscale pipetting for controlled chemistry in small arrayed water droplets using a double-barrel pipet, Nano Lett. 2 (2006) 252–257.
[27] H. Matsuoka, S. Shimoda, Y. Miwa, M. Saito, Automatic positioning of a microinjector in mouse ES cells and rice protoplasts, Bioelectrochemistry 69 (2006) 187–192.
[28] T. Yasukawa, T. Kaya, T. Matsue, Dual imaging of topography and photosynthetic activity of a single protoplast by scanning electrochemical microscopy, Anal. Chem. 71 (1999) 4637–4641.
[29] A.R. Marchand, E. Pearlstein, A simple dual pressure–ejection system and calibration method for brief local application of drugs and modified salines, J. Neurosci. Methods 60 (1995) 99–105.
[30] O. Feinerman, E. Moses, A picoliter fountain-pen, using co-axial dual pipettes, J. Neurosci. Methods 127 (2003) 75–84.
[31] C.C. Park, H. Zhang, M. Pallavicini, J.W. Gray, F. Baehner, C.J. Park, M.J. Bissell, β1 integrin inhibitory antibody induces apoptosis of breast cancer cells, inhibits growth, and distinguishes malignant from normal phenotype in three dimensional cultures and in vivo, Cancer Res. 66 (2006) 1526–1535.
[32] Y. Torisawa, Y. Nashimoto, T. Yasukawa, H. Shiku, T. Matsue, Regulation and characterization of the polarity of cells embedded in reconstructed basement matrix using three-dimensional micro-culture system, Biotechnol. Bioeng. 97 (2007) 615–621.
[33] V.M. Weaver, O.W. Petersen, F. Wang, C.A. Larabell, P. Briand, C. Damsky, M.J. Bissell, Reversion of the malignant phenotype of human breast cells in three-dimensional culture and in vivo by integrin blocking antibodies, J. Cell. Biol. 137 (1997) 231–245.
[34] J. Debnath, S.K. Muthuswamy, J.S. Brugge, Morphogenesis and oncogenesis of MCF-10A mammary epithelial acini grown in three-dimensional basement membrane cultures, Methods 30 (2003) 256–268.
[35] Y. Nashimoto, Y. Takahashi, T. Yamakawa, Y. Torisawa, T. Yasukawa, T. Ito-Sasaki, M. Yokoo, H. Abe, H. Shiku, H. Kambara, T. Matsue, Measurement of gene expression from single adherent cells and spheroids collected using fast electrical lysis, Anal. Chem. 79 (2007) 6823–6830.

—Mini Review—

Morphological Evaluation and Measurement of the Respiration Activity of Cumulus-oocyte Complexes to Assess Oocyte Quality

Haruo Murakawa[1]*, Nobuya Aono[1], Takayuki Tanaka[1], Hiroyuki Kikuchi[1], Hidemune Yoshida[1], Hiroaki Yoshida[1], Masaki Yokoo[2] and Hiroyuki Abe[3]

[1]*Reproductive Research Center, Yoshida Ladies Clinic, Sendai 981-1105, Japan*
[2]*Innovation of New Biomedical Engineering Center, Tohoku University, Sendai 980-8574, Japan*
[3]*Graduate School of Science and Engineering, Yamagata University, Yonezawa 992-8510, Japan*

Abstract: *Scanning electrochemical microscopy (SECM) is a non-invasive and sensitive technique for measuring cellular respiration. In this paper, we review the SECM technique, to establish it as an accurate method for measuring the respiratory activity of single cumulus-oocyte complexes (COCs) and oocytes in animals as well as in humans. Oxygen consumption rates of COCs are influenced by the surrounding cumulus volume and the mitochondrial activity of the cumulus cells. An increase in the oxygen consumption rate was found in bovine oocytes, whereas the oxygen consumption of human oocytes tends to decrease during in vitro maturation (IVM). To analyze the metabolic activity of mitochondrial respiration, ATP content and mitochondrial distribution in bovine oocytes have been examined. An electron microscopic study confirmed mitochondrial reorganization in bovine oocytes during oocyte maturation. These results show that the respiratory activity of oocytes changes with maturation status during IVM and mitochondrial reorganization may partly influence respiratory activity. The SECM procedure is therefore a useful technique for evaluating the metabolic activity and quality of oocytes and cumulus cells in the IVM process.*

Key words: *Cumulus cells, Oocyte maturation, Mitochondria, Oxygen consumption, Electrochemical measurement*

Received: January 7, 2009
Accepted: February 26, 2009
*To whom correspondence should be addressed.
e-mail: repro@yoshida-lc.jp

Introduction

The *in vitro* maturation (IVM) of human oocytes is an attractive technique that provides a patient-friendly approach to assisted reproductive technology. IVM is relatively simple with a shorter period of treatment and lower costs than conventional *in vivo* fertilization (IVF). For anovulatory patients with polycystic ovaries (PCO), a decrease in the dose of ovarian stimulating drugs lowers the risk of ovarian hyperstimulation syndrome. IVM has been successfully applied to animals [1, 2]. Cha *et al.* were the first group to show the success of IVM in human beings using immature donor oocytes retrieved from antral follicles [3]. Recent studies have demonstrated that the results from IVM are comparable to those achieved with contemporary IVF [4, 5]. The applicability and development of IVM technology is dependent on the improvement of *in vitro* culture systems. During *in vitro* culture, cumulus cells play an important role in oocyte maturation. If provided with the several factors that are essential for normal nuclear and cytoplasmic maturation, oocytes can mature and develop to an embryo after fertilization [6]. Therefore, an appropriate evaluation of cumulus-oocyte complexes (COCs) is indispensable for evaluating the quality of oocytes and improving of the results of IVM.

Over the years, several approaches have been used to evaluate COCs. Morphological evaluation is the main technique used to assess COC quality and to predict the subsequent maturation of oocytes in the IVM process. However, morphological evaluations are subjective and difficult, especially for COCs with

intermediate morphological qualities. Therefore, more objective evaluation criteria are needed. Previous studies have suggested that a greater understanding of the metabolic respiration of cumulus cells might yield new strategies for evaluating the quality of bovine oocytes [7, 8]. In this paper we describe the morphological evaluation of COCs and the application of a novel cell respiration measuring system using scanning electrochemical microscopy (SECM) to the assessment of the metabolic activity of cumulus cells and oocytes in bovine and human specimens.

Morphological Evaluation of Cumulus-oocyte Complexes and Oocytes

An appropriate evaluation of COCs is indispensable for the improvement of the IVM system, because cumulus cells play an important role in oocyte quality. For a morphologically precise evaluation of human COCs, size of an oocyte is an important parameter. The precise evaluation of human COCs is needed to predict the competence of oocyte maturation. Prior research has indicated that the diameter of immature oocytes is one of most reliable parameters for predicting oocyte quality. Eppig and Schroeder reported that mice oocytes isolated from females younger than 13 days of age are capable of spontaneous break down of the germinal vesicle (GVBD) when the mean diameter is greater than 60 μm [9]. In a study of porcine immature oocyte, progression to metaphase II was observed in 40% of oocytes that were over 110 μm in diameter, whereas no oocyte less than 90 μm in diameter resumed meiosis [10]. In rhesus monkey oocytes, in which meiotic competence occurs late during oocyte development, oocyte diameters appear relatively constant as the competence to undergo GVBD increases. These phenomena suggest that there is no association between oocyte diameter and maturation [11].

In comparison to animal systems, little is known about humans. Based on data from unstimulated polycystic ovary syndrome (PCOS) patients, Cavilla *et al.* deduced that an oocyte diameter of 81 μm at the time of retrieval was the threshold for GVBD, whereas oocytes of more than 103 μm would mature to metaphase II [12]. They also noted that, during *in vitro* human oocyte maturation, an increase in the average diameter of only 3 μm (from 106 to 109) represents a large change in the cytoplasmic volume (increasing an astonishing 8% during culture), suggesting that oocyte diameter provided valuable information about oocyte potential during IVM. In a proposal for the precise evaluation of human immature oocytes, the two-dimensional area of a depiction image was calculated using image analysis software "Image J".

Another important parameter of oocyte morphological quality is the volume of the human cumulus mass. During IVM, cumulus cells are known to maintain the oocyte nucleus at the GV stage [13]. Expanded human cumulus-oocyte complex patterns have a higher expression of LH receptor mRNA and are associated with more efficient oocyte maturation [14]. Early reports supported the idea that cumulus expansion during IVM improves the developmental capacity [15, 16]. In mice, the fertilization rate of IVM matured oocytes is correlated with the quantity and quality of the expanded cumulus mass [17]. The mechanical loss or spontaneous loss of cumulus cells from COCs has been shown to correlate with a loss of fertilizability [18]. Therefore, the quantity of cumulus mass is a factor influencing the success of IVM. For the morphological classification of cumulus mass, some researchers have separated the cumulus patterns into multilayered and expanded [19, 20].

In this review, we have estimated the multilayered and expanded cumulus mass as the consecutive change and made objective evaluations utilizing an image analysis software program. The COC area was calculated by tracing the edge of the cumulus mass. If the edge was not clear (usually observed in the expanded cumulus mass), the image was analyzed using an edge enhancement mode. The multiple layer formation of the cumulus mass was presented as the C-ratio (area of COC / area of immature oocyte). For the morphological evaluation of human COCs, forty-two human COCs, retrieved from eight women with the PCOS during an IVM program, were used. All COCs were aspirated 36 hours post-hCG between the 10th and 12th day of the menstrual cycle and cultured for 26 hours in TCM199 medium with 10% patient serum, 100 IU/L human chorionic gonadotropin and 75 IU/L follicle stimulating hormone under an atmosphere of 5% CO_2, 5% O_2, and 90% N_2. The parameters analyzed were (1) *Area*; area of the immature oocyte and (2) *Layer*; multiple layer formation of the cumulus mass, presented as the C-ratio. As shown in Fig. 1, these two morphological parameters were compared between the immature (germinal vesicle: GV or metaphase I: MI) and mature (metaphase II: MII) oocyte groups after *in vitro* culture. In the *Area* comparison, the mean level of *Area* was significantly higher in the mature group (8,886 ± 184 vs. 9,806 ± 161, Mean ± SEM, $P < 0.05$). In the

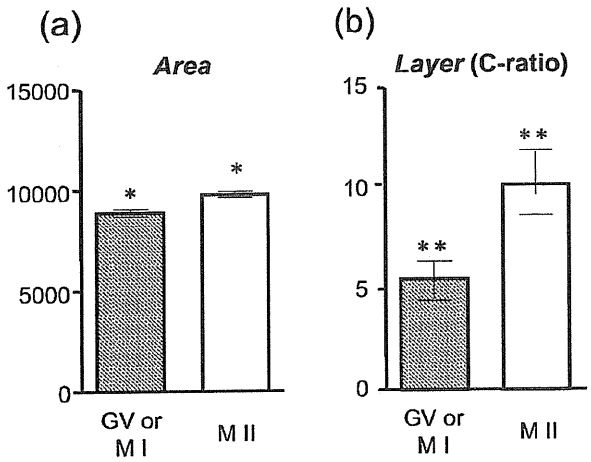

Fig. 1. Comparison of morphological parameters of human immature oocyte and COCs. a: *Area*, Area of immature oocyte; b: *Layer*, Multiple layer formation of cumulus mass was evaluated as C-ratio (Area of COC / Area of immature oocyte). Area and Layer were analyzed before *in vitro* culture and compared prospectively between mature (MII) and immature (MI or GV) group. *, **: significantly different ($P < 0.05$).

Layer comparison, the mean level of the C-ratio was significantly higher in the mature group (5.8 ± 0.8 vs. 10.3 ± 1.6, Mean ± SEM, $P < 0.05$). These results suggest the C-ratio is a useful parameter for predicting the maturation status of oocytes in the IVM process.

Subsequently, we examined the relationship between the cumulus mass morphology and the oocyte quality. Human COCs were classified into five grades based on cumulus mass morphology as follows: Grade 1 (G1), cumulus cells with multi-layers covering the whole oocyte, and a regular round oocyte; Grade 2 (G2), cumulus cells with multi-layers (less than three layers), covering the whole oocyte and a regular round oocyte; Grade 3 (G3), regular round oocytes with cumulus cells covering half of the domain; Grade 4 (G4), naked oocytes without cumulus mass; Grade 5 (G5), naked and irregular shaped oocytes (Fig. 2). High maturation rates of immature oocytes were detected in G1 and G2 (70.0% and 64.3%, respectively) in contrast to the lower maturation rate of 17.7% (mean percentage from G3 to G5).

Cumulus cells are a production site of steroids, growth factor, proteins and other compounds that contribute to cytoplasmic maturation of oocytes. Beneficial effects of cumulus cells on microtubule dynamics and/or chromatin stability, oocyte maturation and early embryonic development have been reported in many species, including humans [21–23]. Cumulus cells are also known to play an important role in the regulation of the meiotic progression of oocytes. During the growth and development of meiotic competence of an oocyte, the cumulus cells are responsible for maintenance of nuclear arrest at the germinal vesicle (GV) stage by transfer of an inhibitory signal through gap junctions which elevates the intracellular cyclic adenosine monophosphate (cAMP) level in the oocytes

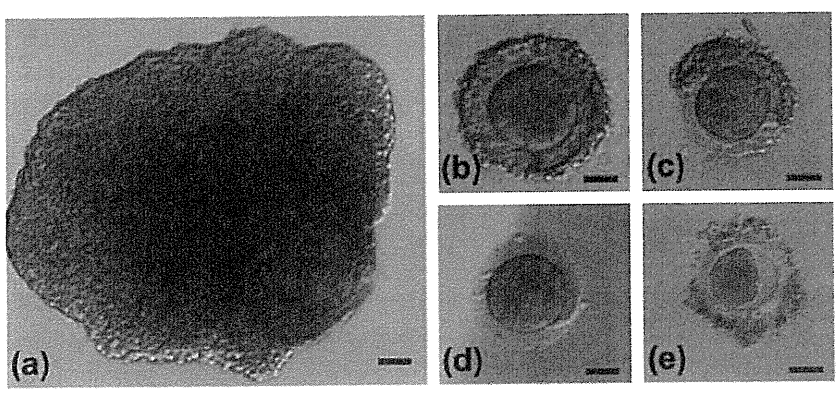

Fig. 2. Light micrographs of human COCs classified by morphological evaluation. (a) Grade 1, cumulus cells with multi-layers covering the whole oocyte, and a regular round oocyte; (b) Grade 2, cumulus cells with multi-layers (less than three layers), covering the whole oocyte and a regular round oocyte; (c) Grade 3, regular round oocytes with cumulus cells covering half of the domain; (d) Grade 4, naked oocytes without cumulus mass; (e) Grade 5, naked and irregular shaped oocytes. Bars = 20 μm.

[24, 25]. Although the precise regulation mechanism of meiotic progression is still controversial [26], it has been suggested that well-developed cumulus cells have the capacity to regulate appropriate maturation and the development of immature oocytes.

Evaluating the Quality of Embryos and Oocytes with Measurement of Respiration Activity with an Electrochemical Measuring Technique

The metabolic activity of embryos and oocytes has been determined from the consumption of nutrients, such as glucose, pyruvate and amino acids [27–30]. Oxygen consumption is an idea indicator of overall metabolic activity because adenosine triphosphate (ATP) is predominantly generated by oxidative phosphorylation, a process in which oxygen plays an essential role [31–33]. Oxygen consumption by embryos and oocytes has been studied with various measuring techniques, such as the Cartesian diver [34, 35], spectrophotometry [36, 37], ultrafluorescence measurements [38, 39], and self-referencing microelectrodes [40–43].

Electrochemical measurement using scanning electrochemical microscopy (SECM) is a technique in which the tip of a microelectrode monitors the local distribution of electro-active species, such as oxygen near the sample surface [44]. This technique can measure the concentration profile of a metabolic product around a spherical sample, such as an embryo, with a probe microelectrode. We have employed the SECM technique to examine oxygen consumption by single embryos [45]. Using a modified SECM measuring procedure, we quantified the respiration activity of embryos in several animal species including humans [46]. SECM can non-invasively measure the respiration activity of single embryos from livestock, such as cattle and pigs, as well as those from small rodents, all with high reproducibility. We recently demonstrated that bovine embryos with high oxygen consumption are better candidates for further development into good quality embryos and yielded higher pregnancy rates after embryo transfer. The respiration activity correlates with the embryo quality. SECM is a highly sensitive and non-invasive method for measuring cellular respiration and may be a valuable tool for accurately assessing the quality of embryos, which could contribute to improved outcomes in assisted reproduction, including human IVF. On the other hand, an accurate method for evaluating the respiratory activity of oocytes remains to be developed.

Table 1. Oxygen consumption rates ($F \times 10^{14}$/mol · s^{-1}) of bovine COCs and denuded oocytes in oocyte maturation cultures

Maturation status	COC (n)	Oocyte (n)
Immature	5.48 ± 0.82 (16)[a]	0.67 ± 0.02 (16)[c]
Mature	3.15 ± 0.42 (20)[b]	1.10 ± 0.05 (20)[d]

Values with different superscripts in each column differ significantly ($P < 0.05$).

Oocyte quality could be the most important factor in determining successful fertilization and embryo development. Therefore, we attempted to establish an evaluation system for oocyte quality based on the respiratory activity of oocytes.

In previous studies, we evaluated the SECM technique, to establish an accurate method for measuring the respiratory activity of single bovine and porcine oocytes [8, 48]. With the SECM procedure, oxygen consumption of bovine COCs and denuded oocytes was monitored (Table 1). Oxygen consumption rates ($\times 10^{14}$/mol · s^{-1}) of immature COCs and oocytes (immediately after recovery from an ovary) were 5.48 and 0.67, respectively. Although the respiration rate of denuded oocytes was lower than that of cumulus cells, the oxygen consumption rate by a single bovine oocyte was quantitatively measured by SECM.

Oxygen consumption has been monitored in COCs and oocytes cultured in serum-free medium for oocyte maturation. An increase in the oxygen consumption rate was found in oocytes [1, 10], whereas the oxygen consumption by COCs [3, 15] decreased during IVM. To analyze the metabolic activity of mitochondrial respiration, the ATP content and mitochondrial distribution in oocytes were examined. The ATP content of oocytes after maturation culture was significantly higher than that of immature oocytes (Fig. 3). In immature oocytes, staining with MitoTracker Orange revealed mitochondrial clumps with a strong signal in the periphery of the cytoplasm (Fig. 4). After IVM, the mitochondrial clumps were located more toward the center of the cytoplasm. An electron microscope study confirmed mitochondrial reorganization in bovine oocytes during oocyte maturation (Fig. 5). These results show that the respiratory activity of bovine oocytes increases during IVM and mitochondrial reorganization may thus be partly due to the respiratory activity. Therefore, we consider the SECM procedure is a useful technique for evaluating the metabolic activity and quality of single oocytes.

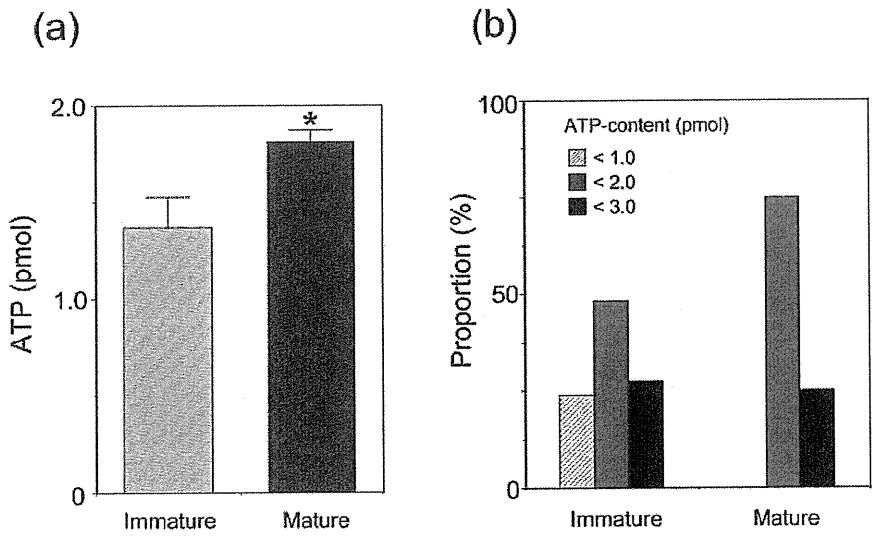

Fig. 3. (a) The ATP content and (b) proportion of oocytes categorized by ATP content: immature and mature bovine oocytes. *: significantly different ($P < 0.05$).

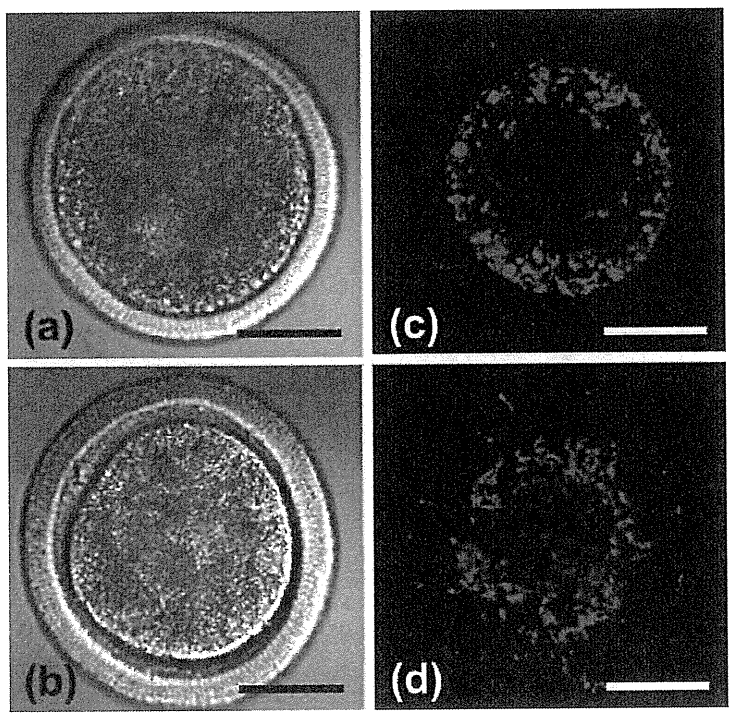

Fig. 4. Midline confocal sections of (a, b) immature and (c, d; cultured in IVMD101 medium) mature bovine oocytes stained by MitoTracker orange. Bars = 50 μm.

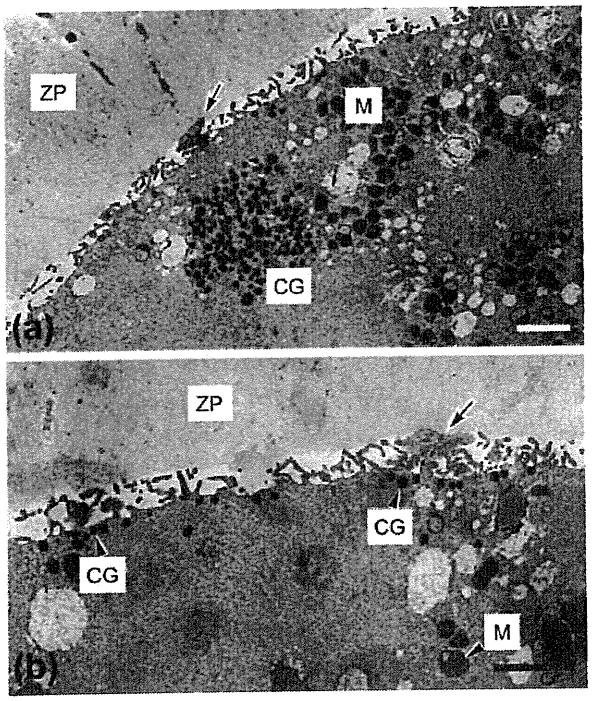

Fig. 5. Electron micrographs of (a) immature and (b) cultured in serum-free maturation medium mature oocytes. a: Many aggregates of mitochondria (M) and cortical granules (CG) were present in the cortex cytoplasm. b: Cortical granules were distributed in the periphery of the cytoplasm, but aggregates of mitochondria were not found. ZP, zona pellucida. Arrows: microvilli. Bars = 2 μm.

Measuring the Respiration Activity of Human COCs and Oocytes

In this part, we review the respiration activity of human COCs and oocytes. Eighty-five human COCs retrieved from eighteen women with the PCOS during an IVM program were examined. Informed consent for the use of the COCs in this study was obtained from all the patients. Thirteen of the eighteen women were administered a short course of follicular stimulating hormone (FSH) and five women accomplished an IVM program without the use of FSH before hCG administration. All COCs were aspirated 36 h post-hCG between the 10th and 12th day of the menstrual cycle and cultured 26 h in TCM199 medium with 10% patient serum, 100 IU/L human chorionic gonadotropin and 75 IU/L follicle stimulating hormone under an atmosphere of 5% CO_2, 5% O_2, and 90% N_2. Cellular unevenness of the cumulus mass has an influence on SECM measurement results. Therefore,

Table 2. Oxygen consumption rates ($F \times 10^{14}$/mol · s^{-1}) of human COCs classified by morphological evaluation

Category	Pre-culture (n)	Post-culture (n)
G1	7.79 ± 1.00 (50)	6.11 ± 0.74 (50)
G2	1.46 ± 0.15 (25)	1.63 ± 0.33 (25)
G3	1.26 ± 0.35 (8)	1.60 ± 0.55 (8)
G4	0.86 ± 0.30 (2)	0.79 ± 0.11 (2)
G5	0.77 (1)	0.35 (1)

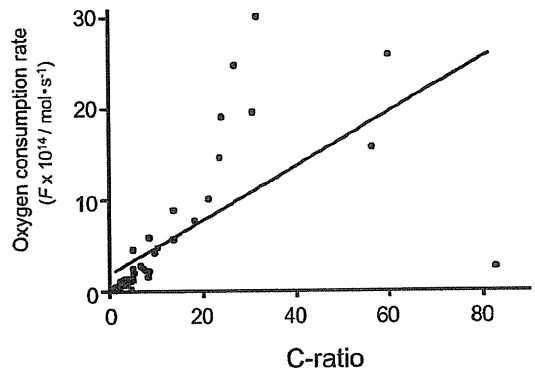

Fig. 6. Correlation between oxygen consumption rate and C-ratio.

the oxygen consumption rate was measured three times for each COC and the mean was used as the measured value.

Relationship between the oxygen consumption rates and morphological categories of human COCs in the pre-culture and post 26 hours-culture stages is shown in Table 2. A linear correlation between the oxygen consumption rate and the C-ratio was shown in Fig. 6 (correlation coefficient: $r^2 = 0.423$, $P < 0.01$). The respiration activity measured by SECM showed that the respiration activity of human COCs with multi-layer cumulus cells (G1) was higher than in the other categories (G2–G5). Ultrastructual studies revealed that the cumulus cells in G1 COCs, which showed high respiration activity, contained many well-developed mitochondria. In contrast, undeveloped mitochondria were scattered in the cumulus cells in G3 COCs (Fig. 7). These results suggest that respiration rates are directly influenced by the surrounding cumulus volume and mitochondrial activity in cumulus cells.

A comparison of the oxygen consumption fluctuation between the pre-culture stage and after 26 hours of culture is shown in Fig. 8. In the FSH administration group, the mean oxygen consumption rate tended to

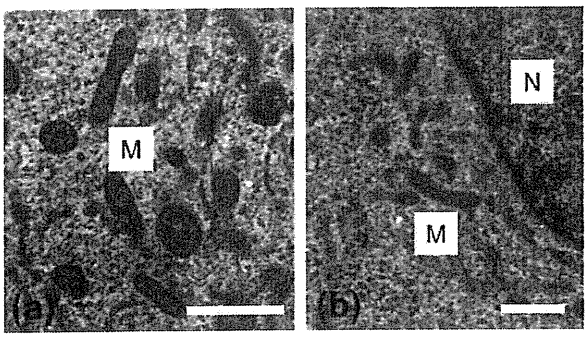

Fig. 7. Electron micrographs of human cumulus cells. Many well-developed mitochondria (M) are present in the cumulus cells of the Grade 1 COC (left image). In contrast, mitochondria showing small size are scattered in the cumulus cells of the Grade 3 COC. N: Nucleus. Bars = 1 μm.

decrease after 26 h of culture (5.62 ± 0.83 vs. 4.25 ± 0.58). In contrast, the mean oxygen consumption rates were similar between the two stages in the non-FSH administration group (4.07 ± 1.19 vs. 4.17 ± 1.02). There was no clinical advantage gained by extending the FSH pre-treatment from 3 to 6 days to produce follicles more than 10 mm in diameter [49]. On the other hand, Wynn *et al.* demonstrated a higher maturation rate in a FSH treatment group [50]. In their study, the maturation rate to metaphase II was higher in the FSH administration group (68.3% vs. 61.3%, in comparison to the non-FSH administration group, unpublished data). The benefit of FSH pre-treatment remains controversial and the development competence cannot be evaluated because of the limitations of the current study protocol.

The efficacy of the administration of hCG remains controversial. In hCG protocol, all patients are administered hCG before oocyte retrieval. After the LH surge, oocytes resume the first meiotic division and enter the second division [51]. At the same time, cumulus mass begins to change to the expanding form. Cumulus expansion may influence a variety of fundamental developmental changes which occur during fertilization. Regarding the use of hCG in bovine, the cumulus cells from antral follicles as small as 5 mm have mRNA transcripts for LH receptors and may respond to hCG stimulation [52]. This finding provides evidence of a mechanism by which hCG begins the maturation process of small antral oocytes *in vivo* and facilitates the completion of meiosis *in vitro*. Chian *et al.* demonstrated that the percentage of oocytes achieving maturation after 48 h *in vitro* culture was significantly higher in the hCG-primed group than in the non-hCG-primed group during human IVM-IVF [53].

Finally, the results of the respiration measurement of single human oocytes using a SECM system are listed in Table 3. The oxygen consumption rate of pre-cultured oocytes (GV stage) was 0.49 × 10^{14}/mol · s^{-1},

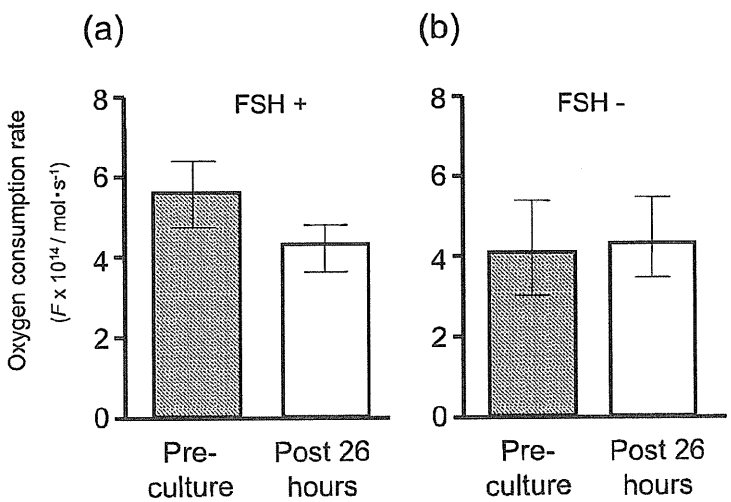

Fig. 8. Comparison of oxygen consumption with or without FSH administration at the pre-culture stage and after 26 h of culture. (a) oxygen consumption rate in the FSH administered group and (b) in the non-FSH administered group.

Table 3. Oxygen consumption rates ($F \times 10^{14}$/mol · s^{-1}) of human denuded oocytes in oocyte maturation cultures

Maturation status	Oxygen consumption rate (n)
GV (Pre-culture)	0.49 ± 0.07 (10)
GV or MI (Post-culture)	0.40 ± 0.21 (19)
MII (Post-culture)	0.41 ± 0.15 (30)

whereas the oxygen consumption rate tended to decrease in matured MII oocytes (0.41 × 10^{14}/mol · s^{-1}). These results suggest that the respiration activity of human oocytes changes with maturation status of oocytes, although the mechanism of this fluctuation needs to be confirmed with further studies.

Conclusions

The SECM technique is a non-invasive and sensitive method for measuring the oxygen consumption of individual COCs and oocytes in animal species including humans. The respiration activity of COCs is directly influenced by the surrounding cumulus cell volume and the mitochondrial activity of cumulus cells. Biochemical and cytological studies strongly suggest that oxygen consumption is an important parameter for evaluating the competence of oocyte maturation. It may be feasible to monitor the profile of an oocyte's mitochondrial activity by measureing its oxygen consumption, and select the oocytes that can sustain fertilization and the development of embryos. Therefore, the SECM technique may have a future in clinical application as a predictor of oocyte quality which could be used for determining to develop into good quality embryos.

Acknowledgements

This work was supported by Research and Development Program for New Bio-Industry Initiatives, Bio-oriented Technology Research Advancement Institution (BRAIN), Grant-in-Aid for Scientific Research (17380164), on Priority Areas "Lifesurveyor" (19021006) from the Ministry of Education, Culture, Sports, Science and Technology of Japan, Special Coordination Funds for Promoting Science and Technology of Japan, and the Japan Livestock Technology Association.

References

1) Blondin, P., Bousqent, D., Twagiramungu, H., Barnes, F. and Sirand, M.A. (2002): Manipulation of follicular development to produce developmentally competent bovine oocyte. Biol. Reprod., 66, 38–43.
2) Barnes, F.L. and Sirard, M.A. (2000): Oocyte maturation. Semin. Reprod. Med., 18, 123–131.
3) Cha, K.Y., Koo, J.J., Ko, J.J., Choi, D.H., Han, S.Y. and Yoon, T.K. (1991): Pregnancy after in vitro fertilization of human follicular oocytes collected from nonstimulated cycles, their culture in vitro and their transfer in a donor oocyte program. Fertil. Steril., 55, 109–113.
4) Le Du, A., Kadoch, I.J., Bourcigaux, N., Doumerc, S., Bourrier, M.C., Chevalier, N., Fanchin, R., Chian, R.C., Tachdjian, G., Frydman, R. and Frydman, N. (2005): In vitro maturation for the treatment of infertility associated with polycystic ovarian syndrome: the French experience. Hum. Reprod., 20, 420–424.
5) Soderstrom-Anttila, V., Makinen, S., Tuuri, T. and Suikkari, A.M. (2005): Favorable pregnancy results with insemination of in vitro matured oocytes from unstimulated patients. Hum. Reprod., 20, 1534–1540.
6) Nagai, T. (2001): The improvement of in vitro maturation systems for bovine and porcine oocytes. Theriogenology, 55, 1291–1301.
7) Abe, H., Saito, T., Shiku, H., Yokoo, M., Itoh-Sasaki, T., Hoshi, H. and Matsue, T. (2006): Analysis of respiratory activity of single bovine oocytes by scanning electrochemical microscopy. In: Proceeding of the 4th International Forum on Post-genome Technologies, pp. 19–22.
8) Abe, H., Shiku, H., Aoyagi, S., Matsue, T. and Hoshi, H. (2006): Oxygen consumption of bovine cumulus cells and oocytes cultured in different culture systems for oocyte maturation. Reprod. Fertil. Dev., 18, 267.
9) Eppig, J.J. and Schroeder, A.C. (1989): Capacity of mouse oocytes from preantral follicles to undergo embryogenesis and development to live young after growth, maturation and fertilization in vitro. Biol. Reprod., 41, 268–276.
10) Hirao, Y., Nagai, T., Kubo, M., Miyano, T., Miyake, M. and Kato, S. (1994): In vitro growth and maturation of pig oocytes. J. Reprod. Fertil., 100, 333–339.
11) Schramm, R.D., Tennier, M.T., Boatman, D.E. and Bavister, B.D. (1993): Chromatin configuration and meiotic competence of oocytes are related to follicular diameter in non-stimulated rhesus monkeys. Biol. Reprod., 48, 349–356.
12) Cavilla, J.K., Kennedy, C.R., Byskov, A.G. and Hartshorne, G.M. (2008): Human immature oocytes grow during culture for IVM. Hum. Reprod., 23, 37–45.
13) Dekel, N. and Beers, W.H. (1980): Development of the rat oocyte in vitro: Inhibition and induction of maturation in the presence or absence of the cumulus oophorus. Dev. Biol., 75, 247–254.
14) Yang, S.H., Son, W.Y., Yoon, S.H., Ko, Y. and Lim, J.H. (2005): colleration between in vitro maturation and

expression of LH receptor in cumulus cells of the oocytes collected from PCOS patients in HCG-primed IVM cycles. Hum. Reprod., 20, 2097–2103.
15) Ball, G.D., Leibfried, M.L., Lenz, R.W., Ax, R.L., Bavister, B.D. and First, N.L. (1983): Factors affecting successful in vitro fertilization of bovine follicular oocytes. Biol. Reprod., 28, 717–725.
16) Naito, K., Fukuda, Y. and Toyama, Y. (1988): Effects of porcine follicular fluid on male pronucleus formation in porcine oocytes matured in vitro. Gamete. Res., 21, 289–295.
17) Chen, L., Russell, P.T. and Larsen, W.J. (1993): Functional significance of cumulus expansion in the mouse: Roles for the preovulatory synthesis of hyaluronic acid within the cumulus mass. Mol. Reprod. Dev., 34, 87–93.
18) Itagaki, Y. and Toyoda, Y. (1991): Factors affecting fertilization in vitro of mouse eggs after removal of cumulus oophorus. J. Mamm. Ova Res., 8, 126–134.
19) Smitz, J., Picton, H.M., Platteau, P., Rutherford, A., Cortvrindt, R., Clyde, J., Nogueira, D., Devroey, P., Lyby, K. and Grondahl, C. (2007): Principal findings from a multicenter trial investigating the safety of follicular-fluid meiosis-activating sterol for in vitro maturation of human cumulus- enclosed oocytes. Fertil. Steril., 87, 949–964.
20) Jurema, M.W. and Noguera, D. (2006): In vitro maturation of human oocytes for assisted reproduction. Fertil. Steril., 86, 1277–1291.
21) Cha, K.Y. and Chian, R.C. (1998): Maturation in vitro of human oocytes for clinical use. Hum. Reprod. Update., 4, 103–120.
22) Goud, P.T., Goud, A.P., Qian, C., Laverge, H., Van der Elst, J., De Sutter, P. and Dhout, M. (1998). In vitro maturation of human germinal vesicle stage oocytes: role of cumulus cells and epidermal growth factor in the culture medium. Hum. Reprod., 13, 1638–1644.
23) Ueno, S., Kurome, M., Ueda, H., Tomii, R., Hiruma, K. and Nagashima, H. (2005): Effects of maturation conditions on spindlemorphology in porcine MII oocytes. J. Reprod. Dev., 51,405–410.
24) Isobe, N. and Terada, T. (2001): Effect of the factor inhibiting germinal vesicle breakdown on the disruption of gap junctions and cumulus expansion of pig cumulus-oocyte complexes cultured in vitro. Reproduction, 121, 249–257.
25) Tanghe, S., Van Soom, A., Nauwynck, H., Coryn, M. and De Kruif, A. (2002): Minireview: Functions of the cumulus oophorus during oocyte maturation, ovulation and fertilization. Mol. Reprod. Dev., 61, 414–424.
26) Guoliang, X., Byskov, A.G. and Anderson, C.Y. (1994): Cumulus cells secrete a meiosis-inducing substance by stimulation with forskolin and cyclic adenosine monophosphate. Mol. Reprod. Dev., 39, 17–24.
27) Rieger, D. (1992): Relationship between energy metabolism and development of early mammalian embryos. Theriogenology, 37, 75–93.
28) Rieger, D., Loskutoff, N.M. and Betteridge, K.J. (1992): Developmentally related changes in the uptake and metabolism of glucose, glutamine and puruvate by cattle embryos produced in vitro. Reprod. Fertil. Dev., 4, 547–557.
29) Rieger, D. and Loskutoff, N.M. (1994): Changes in the metabolism of glucose, puruvate, glutamine and glycine during maturation of cattle oocytes in vitro. J. Reprod. Fertil., 100, 257–262.
30) Gopichandran, N. and Leese, H.J. (2003): Metabolic characterization of the bovine blastocyst, inner cell mass, trophectoderm and blastocoel fluid. Reproduction, 126, 299–308.
31) Thompson, J.G., Partridge, R.J., Houghton, F.D., Cox, C.I. and Leese, H.J. (1996): Oxygen uptake and carbohydrate metabolism by in vitro derived bovine embryos. J. Reprod. Fertil., 106, 299–306.
32) Thompson, J.G., McNaughton, C., Gasparrini, B., McGowan, L.T. and Tervit, H.R. (2000): Effect of inhibitors and uncouplers of oxidative phosphorylation during compaction and blastulation of bovine embryos cultured in vitro. J. Reprod. Fertil., 118, 47–55.
33) Trimarchi, J.R., Liu, L., Porterfield, D.M., Smith, P.J.S. and Keefe, D.L. (2000): Oxidative phosphorylation-dependent and -independent oxygen consumption by individual preimplantation mouse embryos. Biol. Reprod., 62, 1866–1874.
34) Fridhandler, I., Hafez, E.S.E. and Poncus, G. (1957): Developmental changes in the repiratory activity of rabbit ova. Experiments in Cell Research, 13, 132–139.
35) Mills, R.M. and Brinster, R.L. (1967) Oxygen consumption of preimplantation mouse embryos. Exp. Cell Res., 470, 337–344.
36) Magnusson, C., Hillensjo, T., Hamberger, L. and Nilsson, L. (1986): Oxygen consumption by human oocytes and blastocysts grown in vitro. Hum. Reprod., 1, 183–184.
37) Nilsson, B., Magnusson, C., Widehn, S. and Hillensjo, T. (1982): Correlation between blastocyst oxygen consumption and trophoblast cytochrome oxidase reaction at initiation of implantation of delayed mouse blastocysts. J. Embryol. Exp. Morphol., 71, 75–82.
38) Houghton, F.D., Thompson, J.G., Kennedy, C.J. and Leese, H.J. (2000): Oxygen consumption and energy metabolism of the early mouse embryo. Mol. Reprod. Dev., 44, 476–485.
39) Trimarchi, J.R., Liu, L., Smith, P.J.S. and Keefe, D.L. (2000): Noninvasive measurement of potassium efflux as an early indicator of cell death in mouse embryos. Biol. Reprod., 63, 851–857.
40) Land, S.C., Porterfield, D.M., Sanger, R.H. and Smith, P.J.S. (1999): The self-referencing oxygen-selective microelectrode: detection of transmembrane oxygen flux from single cells. J. Exp. Biol., 202, 211–218.
41) Smith, P.J.S., Hammar, K., Porterfield, D.M., Sanger, R.H. and Trimarchi, J.R. (1999): Self-referencing, non-invasive, ion selective electrode for single cell detection of trans-plasma membrane calcium flux. Microsc. Res. Tech., 46, 398–417.
42) Lopes, A.S., Larsen, L.H., Ramsing, N., Lovendahl, P.,

Raty, M., Peippo, J., Greve, T. and Callesen, H. (2005): Respiration rates of individual bovine in vitro-produced embryos measured with a novel, non-invasive and highly sensitive microsensor system. Reproduction, 130, 669–679.

43) Lopes, A.S., Greve, T. and Callesen, H. (2007): Quantification of embryo quality by respirometry. Theriogenology, 67, 21–31.

44) Bard, A.J. and Mirkin, M.V. (2001): Scanning Electrochemical Microscopy, Marcel Dekker Inc., New York.

45) Shiku, H., Shiraishi, T., Ohya, H., Matsue, T., Abe, H., Hoshi, H. and Kobayashi, M. (2001): Oxygen consumption of single bovine embryos probed with scanning electrochemical microscopy. Anal. Chem., 73, 3751–3758.

46) Abe, H., Shiku, H., Aoyagi, S. and Hoshi, H. (2004): In vitro culture and evaluation of embryos for production of high quality bovine embryos. J. Mamm. Ova Res., 21, 22–30.

47) Abe, H. (2007): A non-invaseve and sensitive method for measureing cellular respiration with a scanning electrochemical microscopy to evaluate embryo quality. J. Mamm. Ova Res., 24, 70–78.

48) Yokoo, M., Ito-Sasaki, T., Shiku, H., Matsue, T. and Abe, H. (2008) Multiple analysis of respiratory activity in the identical oocytes by applying scanning electrochemical microscopy. Trans. Materials Res. Soc. JPN., 33, 763–766.

49) Mikkelesen, A.L., Smith, S.D. and Lindenberg, S. (1999): In vitro maturation of human oocytes from regularly menstruating women may be successful without follicle stimulating hormone priming. Hum. Reprod., 14, 1847–1851.

50) Wynn, P., Piction, H.M., Krapez, J.A., Rutherford, A.J., Balen, A.H. and Gosden, R.G. (1998): Pretreatment with follicle stimulating hormone promotes the numbers of human oocytes reaching metaphase II by in vitro maturation. Hum. Reprod., 13, 3132–3138.

51) Sato, E. and Koide, S. (1987): Biochemical transmitters regulating the arrest and resumption of meiosis in oocytes. Int. Rev. Cytol., 106, 1–33.

52) Jin, Z.X., Ock, S.A., Tan, S.L. and Chian, R.C. (2005): What is the smallest size of follicle to respond to human chorionic gonadotropin injestion? Fertl. Steril., 84, S147.

53) Chian, R.C., Buckett, W.M., Turandi, T. and Tan, S.L. (2000): Prospective randomized study of human chorionic gonadotrophin priming before immature oocyte retrieval from unstimulated women with polycystic ovarian syndrome. Hum. Reprod., 15, 165–170.

Biosensors and Bioelectronics 25 (2010) 1723–1728

Contents lists available at ScienceDirect

Biosensors and Bioelectronics

journal homepage: www.elsevier.com/locate/bios

Electrochemical monitoring of hydrogen peroxide released from leucocytes on horseradish peroxidase redox polymer coated electrode chip

Kumi Y. Inoue[a,*], Kosuke Ino[a], Hitoshi Shiku[a], Shigenobu Kasai[b], Tomoyuki Yasukawa[c], Fumio Mizutani[c], Tomokazu Matsue[a,**]

[a] Graduate School of Environmental Studies, Tohoku University, 6-6-11 Aoba, Aramaki, Aoba, Sendai 980-8579, Japan
[b] Department of Environmental Information Engineering, Tohoku Institute Technology, 35-11 Kasumicho, Taihaku, Sendai 982-8588, Japan
[c] Graduate School of Material Science, University of Hyogo, 3-2-1 Kouto, Kamigori-cho, Ako-gun, Hyogo 678-1297, Japan

ARTICLE INFO

Article history:
Received 8 October 2009
Received in revised form
27 November 2009
Accepted 14 December 2009
Available online 21 December 2009

Keywords:
Neutrophils
Osmium wired peroxidase polymer
Reactive oxygen species
Chemiluminescence
Amperometory

ABSTRACT

We developed an electrochemical-sensing device for continuous monitoring extracellular hydrogen peroxide (H_2O_2). The device consists of an indium-tin-oxide electrode coated with osmium-polyvinylpyridine gel polymer containing horseradish peroxidase (Os-HRP) and a poly-dimethyl siloxane well to house the cells on the chip. Granulocyte-like differentiated HL-60 cells were accommodated in the well and stimulated with phorbol 12-myristate 13-acetate (PMA), which triggered the generation of H_2O_2. The extracellular H_2O_2 released from the cells was enzymatically reduced at the Os-HRP-modified electrode chip using Os(II) as an electron donor, resulting in reduction current responses by the device. The reduction current increased immediately upon PMA stimulation and this current transient was similar to that obtained by conventional chemiluminescence assays using sodium luminol. Apocynin, an inhibitor of NADPH oxidase activation, eliminated both the electrochemical and chemiluminescence signals. On the other hand, superoxide dismutase (SOD) increased the amperometric signals and catalase (CAT) decreased, whereas SOD decreased luminescence emission and CAT did not. These results were in accordance with the expected reaction mechanism, and strongly indicate that this new electrochemical-sensing device successfully detects extracellular H_2O_2 production.

1. Introduction

Reactive oxygen species (ROS) are key mediators of the immune and inflammation processes. Leucocytes produce superoxide anion ($^{\bullet}O_2^-$), a primary ROS generated though the activation of NADPH oxidase (Rossi, 1986). $^{\bullet}O_2^-$ is unstable and rapidly disproportioned to hydrogen peroxide (H_2O_2) and oxygen in the presence or absence of superoxide dismutase (SOD) (Griendling and Harrison, 1999). H_2O_2 is relatively stable and permeable through cell membranes. Thus, the noninvasive measurement system, such as electrochemical detection, for H_2O_2 production from the leucocytes can provide essential information in understanding of the immune and inflammation processes. In the research of ROS production of the cells, phorbol myristate acetate (PMA) is widely used for triggering the respiratory burst by mimicking a physiological activator, diacylglycerol, and is known to induce the activation of NADPH oxidase (Hardy et al., 1991). The activation of NADPH oxidase and concomitant ROS production are efficiently inhibited by apocynin, with an IC50 value of 10 μM in activated human neutrophils (Stefanska and Pawliczak, 2008).

Among the enormous studies for the measurement of ROS, luminol-amplified chemiluminescence techniques are widely used for the measurement of ROS because of their high sensitivity and simple handling (Dahlgren and Karlsson, 1999). However, luminol reacts with several ROS including H_2O_2, $^{\bullet}O_2^-$, NO, OH^- and ONO_2^- via complicated reaction pathways to emit chemiluminescent signal (Dahlgren and Karlsson, 1999; S. Kasai et al., 2005; Li et al., 1999; Radi et al., 1993). Of these substrates, the main chemiluminescence activity in respiratory bursts is believed to be derived from $^{\bullet}O_2^-$ (S. Kasai et al., 2005; Lundqvist and Dahlgren, 1996), but it is very difficult to estimate the real contribution of ROS species. Electrochemical techniques have also been employed for real-time detection of the release of ROS from living cells. Amatore et al. (2006) simultaneously detected multiple ROS from a single macrophage using a carbon microelectrode. Pt electrodes have been commonly used for detecting H_2O_2 since Pt shows electrocatalytic activity for the oxidation of H_2O_2 at a potential of approximately +0.7 V vs. Ag/AgCl (Amatore et al., 2006; S. Kasai et al., 2005; Liu and Zweier, 2001). The use of horseradish peroxidase (HRP)-modified electrodes allows us to determine the H_2O_2

* Corresponding author. Tel.: +81 22 795 7281; fax: +81 22 795 6167.
** Corresponding author. Tel.: +81 22 795 7209; fax: +81 22 795 7209.
E-mail addresses: inoue@bioinfo.che.tohoku.ac.jp (K.Y. Inoue), matsue@bioinfo.che.tohoku.ac.jp (T. Matsue).

0956-5663/$ – see front matter © 2009 Elsevier B.V. All rights reserved.
doi:10.1016/j.bios.2009.12.014

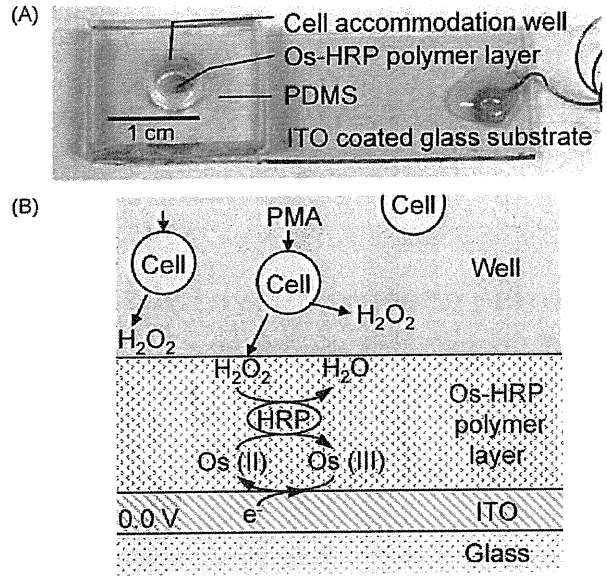

Fig. 1. (A) Photograph of the electrode chip with a PDMS well; (B) schematic illustration of the principle behind the chronoamperometric detection of H_2O_2 produced by living cells using an Os-HRP-modified ITO electrode.

concentration at a lower operational potential (Alpeeva et al., 2005; Ruzgas et al., 1996; Shleev et al., 2008; Crespilho et al., 2008, 2009). The sensitivity for the ROS detection with the electrochemical methods was found to be comparable with that with chemiluminescence methods (S. Kasai et al., 2005; Ashkenazi et al., 2009).

Osmium-polyvinylpyridine gel polymer containing HRP (Os-HRP), invented by Heller and coworkers (Vreeke et al., 1992), has been used for various biosensor elements (Garguilo and Michael, 1994; N. Kasai et al., 2005; Matsuura et al., 2005; Mizutani et al., 2008; Nakajima et al., 2003; Vreeke et al., 1992) because of its high sensitivity for the electrochemical detection of H_2O_2 at a lower operational potential. Electrodes modified with the polymer show high current densities, high sensitivity for H_2O_2, and low oxygen interference owing to effective electrical communication between the HRP (redox enzyme) and Os (electron transfer mediator) (Vreeke et al., 1992). Covalent attachment of the redox enzyme and electron transfer mediator to the electrode surfaces also allows the bioactivity of living cells to be reliably monitored, since attachment prevents signal degradation caused by the unexpected uptake of enzymes and mediators by cells. Heller et al. developed an Os-polyvinylpyridine gel polymer containing glucose oxidase (Os-Gox) for the fabrication of glucose-sensing devices. They implanted an Os-Gox-coated electrode into the subcutaneous tissue of a dog for in vivo glucose sensing (Linke et al., 1994). Os-HRP-modified microelectrodes have been used for the detection of choline in the extracellular fluid of rat brain (Garguilo and Michael, 1994) and for real-time imaging of H_2O_2 release from a rat hippocampal slice (N. Kasai et al., 2005).

We report here a new type of electrochemical device consisting of an Os-HRP-modified electrode chip and a polymer well for accommodating cells (Fig. 1A). The device was used to continuously monitor extracellular H_2O_2 released from granulocyte-like differentiated human promyelocytic leukemia HL-60 cells in the well. When the cells were stimulated with phorbol 12-myristate 13-acetate (PMA), the device indicated a significant increase in the amperometric response for H_2O_2 released from the cells (Fig. 1B). We compared amperometric responses with results from the luminol-based chemiluminescence method in the presence of NADPH oxidase inhivitor or ROS scavengers, in order to ensure that this device successfully detects extracellular H_2O_2 production.

2. Experimental

2.1. Materials and reagents

Ethanol, glucose, all-*trans* retinoic acid (RA), sodium luminol (NaLH), PMA, HRP and catalase (CAT) were purchased from Wako Pure Chemical Industries, Ltd. (Japan). RPMI 1640 medium, phosphate buffered saline (PBS) and SOD were purchased from Sigma Chemical Co. (St. Louis, MO, USA), and apocynin was purchased from Calbiochem (Germany). Aqueous solutions were prepared using high-purity distilled and deionized water from a Milli-Q filtration system (Millipore Corporation, USA).

2.2. Cell culture and differentiation

Human promyelocytic leukemia cell line HL-60, originally obtained from Riken Cell Bank (Japan), was maintained in RPMI 1640 medium supplemented with 10% fetal bovine serum (FBS; Hyclone, USA) and 1% penicillin–streptomycin (Invitrogen) in a humidified atmosphere containing 5% CO_2 (Kasai et al., 2006). To induce the differentiation of HL-60 cells to granulocyte-like cells, cells were incubated with 1.0 μM RA for 5 days. A 10 mM RA/99.5% ethanol stock solution was stored at −80 °C. A small aliquot of this solution was added to the growth medium to obtain the desired final concentration of RA, and to lower the ethanol concentration in the medium to eliminate undesired influences on the differentiation and proliferation of HL-60 cells. The differentiated cells were washed and resuspended in PBS supplemented with 1.0 mM glucose (PBS + Glu) for chemiluminescence and electrochemical measurements. The population of living cells was quantified with fluorescence microscopy (IX71; Olympus) using a fluorescent dye, calcein-AM (Dojindo Laboratories, Japan), and the cell suspensions were stored on ice until use.

2.3. Fabrication of PDMS well/Os-HRP ITO device

Fig. 1A shows a photograph of the electrochemical device used in this study. Indium-tin-oxide (ITO) coated glass (1.5 cm × 5.0 cm; Sano Vacuum Industries Co., Ltd., Japan) was cleaned in an oxygen plasma generator (LTA-101, Yanaco Co., Japan) for 30 s. Then, a 1.5-μL aliquot of Os-HRP polymer solution (Bioanalytical Systems, USA) was dropped on the ITO surface. The solution spread over the hydrophilic surface and formed a circular thin film approximately 4.5 mm in diameter after drying at 4 °C overnight. The coated electrode chips were stored at 4 °C in the dark.

For the cell assay, a poly-dimethyl siloxane (PDMS) well/Os-HRP ITO device was fabricated as follows. A PDMS prepolymer (SILPOTW/C, Dow Corning Toray, Japan) was poured on an acrylic master plate and cured in an oven at 90 °C for 30 min, then the PDMS replica was peeled off from the master. The resultant PDMS replica with a cylindric hole (5.0 mm diameter and 5.0 mm height) was placed on the electrode chip and used as a well to accommodate the cells. The PDMS well/Os-HRP ITO device thus fabricated was used for electrochemical monitoring of ROS released from the cells.

In order to confirm the catalytic function of HRP in the polymer layer, we prepared a comparable device but with deactivated HRP. Deactivation was achieved by treating the Os-HRP polymer layer with 15% H_2O_2 for 30 min at room temperature.

2.4. Equipment and methods for electrochemical measurement

All electrochemical measurements were performed using a potentiostat (HSV-100; Hokuto Denko Corp., Japan). Potentials were referenced to an Ag/AgCl sat. KCl electrode, using a gold wire as the counter electrode.

For basic characterization of the electrode chip, a portion of the chip with Os-HRP layer was soaked in 4.5 mL PBS solution. Cyclic voltammetry was conducted at a scan rate of 20 mV/s from −0.1 to +0.6 V at room temperature. Amperometric measurements for calibration of the H_2O_2 signal were performed at an operational potential of 0.0 V; after the current reached steady state at 0.0 V (i.e., almost all the Os was reduced to Os(II)), a 500-μL aliquot of serially diluted H_2O_2 standard solution (Cell Technology Inc., USA) was added to the gently stirred PBS solution containing the chip, and the current transient was monitored.

For the cell assay, the PDMS well/Os-HRP device was maintained at 37 °C on a thermo plate (Tokai Hit, Japan) during preincubation and measurements. Cell suspension (90 μL) containing 1×10^5 cells in PBS + Glu was added to the PDMS well, then a potential of 0.0 V was applied to the ITO electrode. After 10 min incubation, the current reached steady state. Then, a 10-μL aliquot of PMA/PBS-Glu solution was added to the well and the current transient was monitored.

In experiments conducted using NADPH oxidase inhibitor and ROS scavengers, 100 μM apocynin, 250 U/mL SOD or 250 U/mL CAT was added to the cell suspension in a well and incubated for 10 min before PMA stimulation.

2.5. Equipment and methods for chemiluminescence measurements

Chemiluminescence measurements were performed using a highly-sensitive CCD camera (PI-MAX 512RB; Princeton Instruments, USA) placed 30 cm above a sterile black polystyrene 96-well cell culture plate (Nunc) containing samples in a shade box. The 96-well plate was set on a thermo plate (Tokai Hit, Japan) to keep the samples at 37 °C. Cell suspension (150-μL aliquots containing 2×10^5 cells in PBS + Glu) was dispensed into the wells and incubated on the thermo plate for 10 min. Chemiluminescence measurements were started within 5 min of adding a 50-μL aliquot of 37 °C pre-warmed stimulus mixture solution containing PMA, 4 mM LHNa and 16 U/mL HRP in PBS-G. Chemiluminescence images were accumulated for 5 or 15 min. For time course monitoring, chemiluminescence intensities of the images were calculated as total intensities of 40×40 pixels trimed around each well. In experiments conducted using NADPH oxidase inhibitor and ROS scavengers, 100 μM apocynin, 250 U/mL SOD or 250 U/mL CAT was added to the cell suspension in a well and incubated for 10 min before PMA stimulation.

3. Results and discussion

3.1. Characterization of the electrode chip

We performed cyclic voltammetry and amperometry to characterize the basic performance of an Os-HRP-modified ITO electrode without PDMS well and cells. The cyclic voltammogram showed symmetric oxidation and reduction waves without diffusion tails at the potential of 0.36 V. The shapes were consistent with that reported in previous paper (Vreeke et al., 1992). The peak currents increased linearly with the scan rate in the range 4–100 mV/s. These phenomena are typical for surface-confined redox species. The surface concentration of the redox site (Os complex) was calculated from a coulometric analysis of the peaks, and was found to be 7.5×10^{-9} mol/cm^2. The cyclic voltammogram with deactivated HRP was similar to that with active HRP, indicating that the deactivation process does not significantly affect the redox performance of the Os complex. We also observed the chronoamperometric response of the Os-HRP (active)-modified electrode chip at 0.0 V for the successive addition of 1.0 μM H_2O_2 with stirring. On each addition of H_2O_2, the reduction current immediately increased, and then reached steady-state within 10 s. The response current at steady-state increased with increasing concentration of H_2O_2 in the solution. On the other hand, the electrode chip with deactivated HRP showed no response upon addition of H_2O_2. This clearly suggests that treating the electrode chip with 15% H_2O_2 for 30 min completely deactivates the HRP in the polymer, and that H_2O_2 is not directly oxidized or reduced on the electrode surface at 0.0 V even if the Os polymer is confined on the surface.

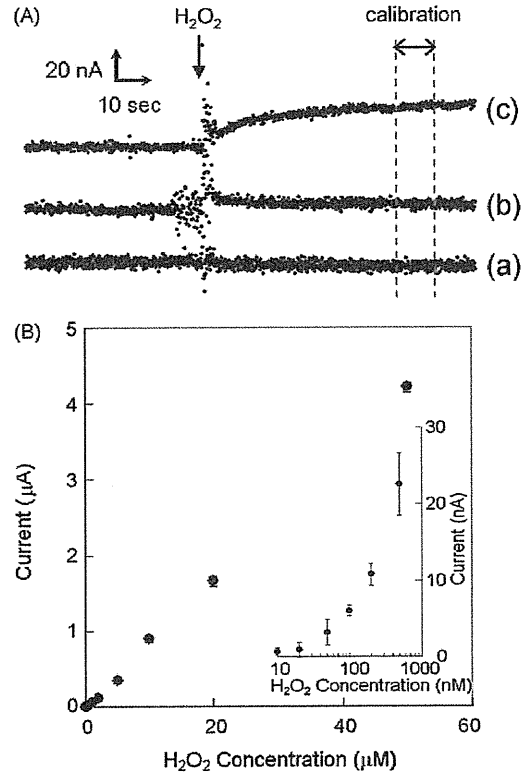

Fig. 2. (A) Typical amperometric response of the electrode chip for standard H_2O_2 solutions at low concentrations. Amperometric measurements were carried out at +0.0 V vs. an Ag/AgCl reference electrode. The concentration of H_2O_2: (a) 0 nM, (b) 50 nM, (c) 500 nM. (B) Calibration curve for the averaged amperometric responses at 50–60 s in (A) against the concentration of H_2O_2. *Inset*: The low concentration part of the calibration curve. Error bars show ±standard deviation ($n = 3$). The coefficient of variations for over 1 μM H_2O_2 were within 10%.

Fig. 2A shows the chronoamperometric responses at low H_2O_2 concentrations. Although the solution stirring caused data scattering, a clear increase in the reduction current was observed after injection of H_2O_2 even at 50 nM H_2O_2. We measured the average currents between 50 and 60 s after H_2O_2 injection to obtain the calibration curve for determining H_2O_2 concentration (Fig. 2B). The reduction current increased linearly with H_2O_2 concentration in the range of 50 nM to 50 μM. The detection range is in good agreement with that reported in a previous study that used a 3-mm carbon disc electrode coated with the same polymer (Vreeke et al., 1992) and also indicates that our device can conduct highly sensitive H_2O_2 detection compared with other electrochemical techniques (Ruzgas et al., 1996).

3.2. Electrochemical and chemiluminescence signal transients in cell measurements depending upon PMA concentration

Using the PDMS well/Os-HRP ITO device, we monitored the electrochemical signal transient originating from ROS released from RA-differentiated HL-60 cells stimulated by various concentrations

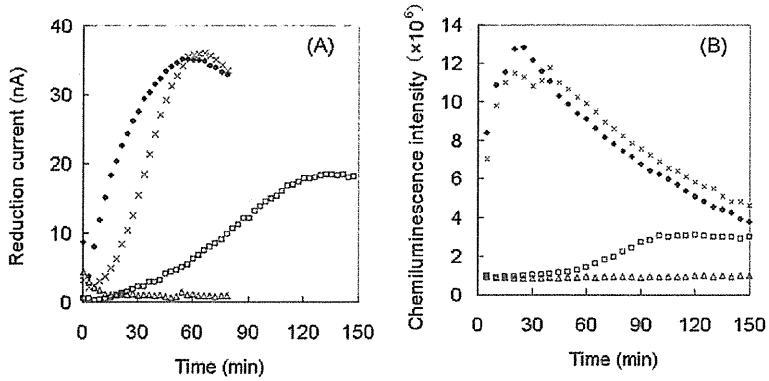

Fig. 3. Typical PMA concentration-dependent time course variation in chronoamperometric responses (A) and chemiluminescence intensities (B). The concentrations of PMA were (●) 10 μg/mL, (×) 1 μg/mL, (□) 0.1 μg/mL, and (△) without PMA. Chemiluminescence intensities were calculated for total intensities of 40 × 40 pixels from 5 min accumulated images. Gain: 250.

of PMA. Fig. 3A shows typical chronoamperometric responses: the reduction currents gradually increased after PMA (0.01–10 μg/mL) was added to the well, and then declined after a period of time. The time required to show the current peak, and the response intensity, tends, respectively, to be shorter and larger as the concentration of PMA for cell stimulation increased. No significant current change was observed without PMA. Fig. 3B shows the time course of chemiluminescence intensities under the same conditions as the electrochemical measurements. The two techniques provide similar results, confirming that the PDMS well/Os-HRP ITO device affords reliable information on ROS production by differentiated HL-60 cells.

3.3. Characterization of the electrochemical signal

To characterize the electrochemical signals, we investigated the effect of apocynin (NADPH oxidase inhibitor), SOD (scavenger of $^{\bullet}O_2^-$) and CAT (scavenger of H_2O_2). HL-60 cells were preincubated in the PDMS well/Os-HRP ITO device with the scavenger or inhibitor. After 10 min preincubation, the cells were stimulated with 1 μg/mL PMA and the reduction current was monitored. Fig. 4A shows the chronoamperometric response under a variety of conditions. The increase in the reduction current in the presence of 100 μM apocynin (Fig. 4A(b)) was less than 20% of that observed in the control experiment (Fig. 4A(a)). This result indicates that more than 80% of the current response originates from the reaction catalyzed by NADPH oxidase:

$$NADPH + 2O_2 \xrightarrow{\text{NADPH oxidase}} NADP^+ + 2{}^{\bullet}O_2^- + H^+ \quad (1)$$

We also employed SOD and CAT as scavengers of $^{\bullet}O_2^-$ and H_2O_2, respectively. SOD catalyzes the dismutation of $^{\bullet}O_2^-$ into O_2 and H_2O_2:

$$2{}^{\bullet}O_2^- + 2H^+ \xrightarrow{SOD} O_2 + H_2O_2 \quad (2)$$

When SOD is added to the cell suspension, the reduction current is expected to increase because additional H_2O_2 would be produced by reaction (1). On the other hand, CAT is expected to reduce the reduction current because it catalyzes the decomposition of hydrogen peroxide into and O_2 and H_2O:

$$2H_2O_2 \xrightarrow{CAT} 2H_2O + O_2 \quad (3)$$

In the presence of 250 U/mL SOD, the reduction current increased immediately after addition of PMA (Fig. 4A(c)), whereas incubation with 250 U/mL CAT suppressed the current increase (Fig. 4A(d)) compared with the control experiment (Fig. 4A(a)). No obvious increases in the reduction current were observed when PMA stimulation was omitted (Fig. 4A(e)), when undifferentiated HL-60 cells with no ROS generation activity (Muranaka et al., 2005) were used (Fig. 4A(f)), or when the device was prepared with deactivated HRP (Fig. 4A(g)). All the above findings indicate that H_2O_2 is the main molecule responsible for the generation of the electrochemical signal by leucocytes.

The initial production rate of H_2O_2 was determined from the initial slope of the current response using the H_2O_2-reduction current response curve shown in Fig. 4A. The initial production rate of H_2O_2 in the presence of 250 U/mL SOD is more than 3 times

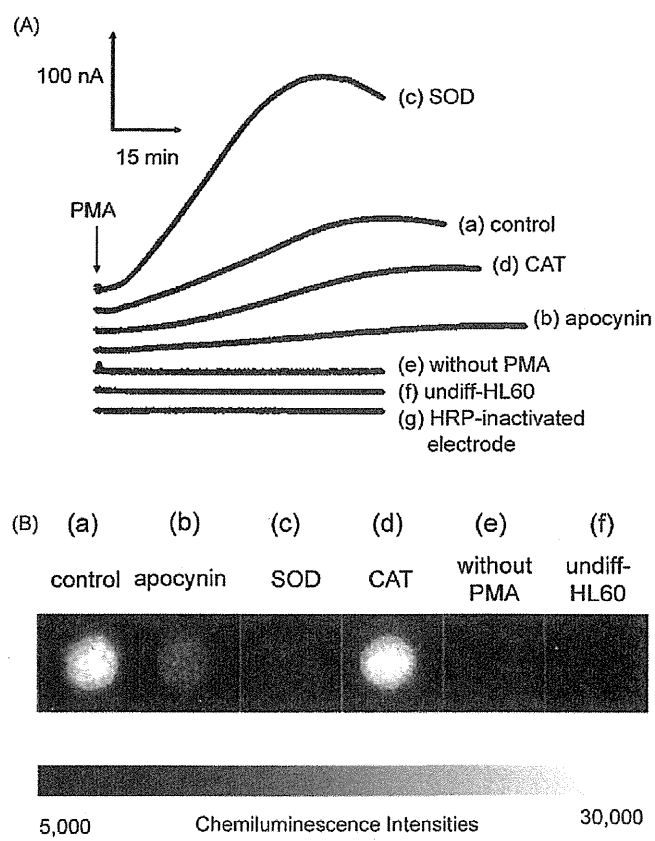

Fig. 4. Typical amperometric response transients (A) and accumulated chemiluminescence images of 30–45 min (B) after stimulation with 1 μg/mL PMA; (a) control, (b) with 100 μM apocynin, (c) with 250 U/mL SOD, (d) with 250 U/mL CAT, (e) without PMA, (f) using undifferentiated HL-60 cells and (g) using an HRP-deactivated electrode.

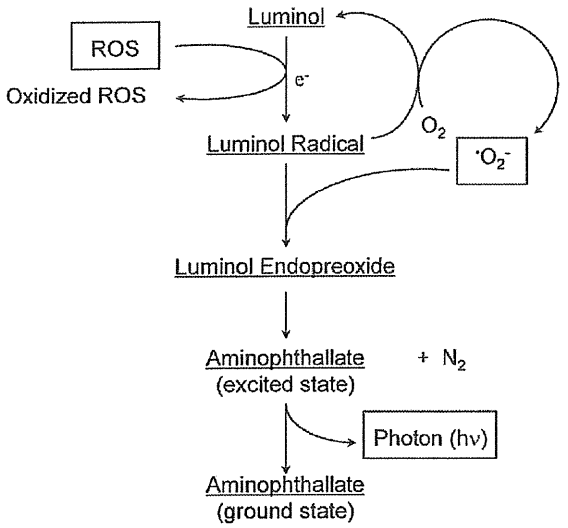

Fig. 5. Scheme of the chemical reaction pathway leading to luminol dependent chemiluminescence with ROS.

larger than that observed in the control measurement. On the other hand, 250 U/mL CAT decreased H_2O_2 production by two-thirds. These results are in good agreement with the predictions based on reactions (2) and (3). H_2O_2 production rates between 10 and 30 min after PMA stimulation were found to be approximately 6, 18 and 4 pmol/min per 1×10^5 cells for without scavenger, with SOD, and with CAT, respectively. The production rates determined in the present study are considerably lower than those reported by Umegaki and Fenech (2000). They reported that granulocyte-like-differentiated HL-60 cells stimulated with 60 ng/mL PMA produced H_2O_2 at 100 pmol/min (phenol red method) and $^{\bullet}O_2^-$ at 300 pmol/min (cytochrome c method) per 1×10^5 cells. Although the reason for the discrepancy is not clear at present, the ratio of the rate with SOD to that without SOD in the present study is 3, which is a reasonable range because 1/2 mol of H_2O_2 is produced from 1 mol of $^{\bullet}O_2^-$ in the presence of SOD (Eq. (2)). For comparison, the ratio reported by Umegaki and Fenech (2000) is 2.5.

3.4. Comparison of chemiluminescence and electrochemical methods

Fig. 4B shows chemiluminescence images of wells with 2×10^5 HL-60 cells under the conditions as the electrochemical measurements in Fig. 4A. The images were obtained 30–45 min after stimulation with 1 μg/mL PMA (15 min accumulated images). Incubation with 100 μM apocynin decreased the chemiluminescence signal (Fig. 4B(b)), and no chemiluminescence was detected from HL-60 cells without PMA stimulation or from undifferentiated HL-60 cell with PMA stimulation. These results agree with those from electrochemical measurements using the PDMS well/Os-HRP ITO device. However, incubations with SOD and CAT gave different results from those obtained electrochemically: the presence of 250 U/mL SOD effectively decreased chemiluminescence (Fig. 4B(c)), and 250 U/mL CAT did not affect the signal (Fig. 4B(d)). The present assay is based on detection of luminol-dependent chemiluminescence, which is also predominantly derived from $^{\bullet}O_2^-$ in respiratory burst (Dahlgren and Karlsson, 1999; S. Kasai et al., 2005). Ashkenazi et al. (2009) reported that 300 U/mL SOD inhibits 90% of isoluminol chemiluminescence activity, but more than doubles the electrochemical signal for H_2O_2. This difference is clearly explained by the reaction mechanisms: electrochemical measurements detect the H_2O_2 produced from the SOD-catalyzed dismutation of $^{\bullet}O_2^-$ (Eq. (2)), whereas the luminol-based chemiluminescence reaction has critical step intermediated by $^{\bullet}O_2^-$ (Fig. 5) (Li et al., 1999). SOD decreases the concentration of $^{\bullet}O_2^-$, thereby reducing chemiluminescence. Electrochemical detection is thus effective for monitoring extracellular H_2O_2, while the chemiluminescence method is suitable for real-time monitoring of ROS generation by cells. H_2O_2 is a key metabolite in oxidative stress and is important in cell signaling cascades (Liu and Zweier, 2001). Thus, a sensing system for monitoring extracellular H_2O_2 is very useful for disclosing oxidative stresses and other intracellular processes. The present device, based on the electrochemical detection of H_2O_2, has advantages for sensitivity, selectivity and quantitation, and will be applicable for a variety of studies dealing with living cells.

4. Conclusion

In this study, we developed an electrochemical device for continuous monitoring extracellular H_2O_2. The device consists of an Os-HRP-modified electrode chip for highly sensitive H_2O_2 detection and a PDMS well for the accommodation of living cells. When granulocyte-like-differentiated HL-60 cells in the well were stimulated with PMA, amperometric responses on the Os-HRP polymer-modified electrode chip were generated, indicating ROS production by the cells. SOD increased the electrochemical response, CAT decreased the response, and apocynin significantly decreased the response. All of these responses can be explained by the intrinsic functions of these species. The results indicate that H_2O_2 is the main molecule contributing to the generation of the electrochemical signal. The present electrochemical detection device is a useful tool for continuous monitoring of H_2O_2 release in respiratory burst and also can be applied to simple and portable whole-cell biosensing systems for inflammatory compounds, and for hazardous materials causing oxidative stresses (Inoue et al., 2008).

Acknowledgements

This work was partly supported by a Grant-in-Aid for Scientific Research (S) (No. 18101006) from the Japan Society for the Promotion of Science (JSPS) and Special Coordination Funds for Promoting Science and Technology, Formation of the Innovation Center for Fusion of Advanced Technologies from the Japan Science and Technology Agency.

Appendix A. Supplementary data

Supplementary data associated with this article can be found, in the online version, at doi:10.1016/j.bios.2009.12.014.

References

Alpeeva, I.S., Niculescu-Nistor, M., Leon, J.C., Csoregi, E., Sakharov, I.Y., 2005. Biosens. Bioelectron. 21, 742–748.
Amatore, C., Arbault, S., Bouton, C., Coffi, K., Drapier, J.C., Ghandour, H., Tong, Y.H., 2006. Chembiochem 7, 653–661.
Ashkenazi, A., Abu-Rabeah, K., Marks, R.S., 2009. Talanta 77, 1460–1465.
Crespilho, F.N., Ghica, M.E., Gouveia-Caridade, C., Oliveira, O.N., Brett, C.M.A., 2008. Talanta 76, 922–928.
Crespilho, F.N., Lanfredi, A.J.C., Leite, E.R., Chiquito, A.J., 2009. Electrochem. Commun. 11, 1744–1747.
Dahlgren, C., Karlsson, A., 1999. J. Immunol. Methods 232, 3–14.
Garguilo, M.G., Michael, A.C., 1994. Anal. Chem. 66, 2621–2629.
Griendling, K.K., Harrison, D.G., 1999. Circ. Res. 85, 562–563.
Hardy, S.J., Robinson, B.S., Poulos, A., Harvey, D.P., Ferrante, A., Murray, A.W., 1991. Eur. J. Biochem. 198, 801–806.
Inoue, K.Y., Yasukawa, T., Shiku, H., Matsue, T., 2008. Electrochemistry 76, 525–528.
Kasai, N., Han, C.X., Torimitsu, K., 2005. Sens. Actuators B Chem. 108, 746–750.
Kasai, S., Shiku, H., Torisawa, Y.S., Noda, H., Yoshitake, J., Shiraishi, T., Yasukawa, T., Watanabe, T., Matsue, T., Yoshimura, T., 2005. Anal. Chim. Acta 549, 14–19.